Microstimulation of sensory cortex engages natural sensory representations

Highlights

- Simulated cortical stimulation engages recurrence-mediated pattern completion

- Optical microstimulation engages recurrently coupled cortical populations

- Pairing microstimulation with sensory input increases representational overlap

Authors

Ravi Pancholi, Andrew Sun-Yan, Simon Peron

Correspondence

speron@nyu.edu

In brief

Pancholi et al. show that direct optogenetic stimulation of vibrissal somatosensory cortex disproportionately engages touch but not whisker movement populations, consistent with recurrence-mediated pattern completion. Repeated optogenetic stimulation paired with natural touch enhances this effect.

CellPress

Article

Microstimulation of sensory cortex engages natural sensory representations

Ravi Pancholi,[1] Andrew Sun-Yan,[1] and Simon Peron[1,2,*]
[1]Center for Neural Science, New York University, 4 Washington Pl., Rm. 621, New York, NY 10003, USA
[2]Twitter: @PeronLab
*Correspondence: speron@nyu.edu
https://doi.org/10.1016/j.cub.2023.03.085

SUMMARY

Cortical activity patterns occupy a small subset of possible network states. If this is due to intrinsic network properties, microstimulation of sensory cortex should evoke activity patterns resembling those observed during natural sensory input. Here, we use optical microstimulation of virally transfected layer 2/3 pyramidal neurons in the mouse primary vibrissal somatosensory cortex to compare artificially evoked activity with natural activity evoked by whisker touch and movement ("whisking"). We find that photostimulation engages touch- but not whisking-responsive neurons more than expected by chance. Neurons that respond to photostimulation and touch or to touch alone exhibit higher spontaneous pairwise correlations than purely photoresponsive neurons. Exposure to several days of simultaneous touch and optogenetic stimulation raises both overlap and spontaneous activity correlations among touch and photoresponsive neurons. We thus find that cortical microstimulation engages existing cortical representations and that repeated co-presentation of natural and artificial stimulation enhances this effect.

INTRODUCTION

Cortical activity occupies a subspace of possible activity patterns.[1-6] For instance, spontaneous activity often resembles activity evoked by natural stimuli, an observation attributed to intrinsic constraints imposed by cortical connectivity and variable physiology among neurons.[7,8] Intrinsic constraints on evoked activity patterns may explain why microstimulation of the sensory cortex can evoke naturalistic sensory perceptions[9] and motor cortical stimulation can drive naturalistic movements.[9,10]

Cortical networks are organized in a highly specific manner. Reciprocal connectivity among small groups of pyramidal neurons exceeds that expected by chance.[11,12] Synaptic connectivity is also heterogeneous, with a few very strong synapses among a larger pool of weak synapses.[13] In layer (L) 2/3 of the mouse primary visual cortex, similarly tuned neurons are more interconnected,[14-17] as are cortical neurons that receive common input from the thalamus[18] or other cortical layers.[19] These observations suggest that the cortex consists of small, highly interconnected subnetworks in a sea of weaker connectivity. Such structured connectivity should favor pattern completion in response to random stimulation.[20]

Cortical microstimulation has been used extensively in the study of perception, with both somatosensory[21] and visual cortical[22,23] stimulation biasing perception. However, due to the difficulties of recording during microstimulation, it remains unclear whether microstimulation engages activity patterns resembling those evoked by natural stimuli, which could account for perceptual biasing. Two-photon optogenetic experiments allow for stimulation of individual opsin-expressing neurons

with known tuning while imaging population activity. These experiments reveal that perception can be biased toward the tuning of the stimulated neurons, predicated on effectively engaging pattern completion.[24,25] Does untargeted cortical stimulation also engage pattern completion? Because optical microstimulation is compatible with concurrent recording, it opens the door to determining whether intrinsic network features constrain experimentally evoked activity by driving it to resemble natural cortical responses, even when stimulation is not targeted to neurons with specific tuning.

Here, we combine optical microstimulation with volumetric two-photon microscopy[26,27] to ask whether directly driven cortical activity engages the same neural populations as naturalistic stimuli. First, we assess the responsiveness of neurons in L2/3 of the primary vibrissal somatosensory cortex (vS1) to vibrissal touch and movement ("whisking"). Next, we assess the response of the same neurons to direct optogenetic stimulation. Because touch but not whisking neurons are recurrently coupled,[28] only touch networks should engage in pattern completion,[20] a prediction borne out by our results.

We next ask whether this effect can be enhanced by repeated co-stimulation of the natural and photoresponsive populations. Hebbian plasticity should drive elevated connectivity among co-stimulated neurons,[29,30] given the spike-timing-dependent plasticity rule governing L2/3 pyramidal neurons in vS1.[31] We therefore expose mice to an induction paradigm in which optical microstimulation of vS1 is paired with concurrent presentation of a vibrissal touch stimulus. We find that this enhances the overlap among the photoresponsive and touch-responsive populations. Our work suggests that intrinsic features of cortical circuitry bias activity toward response patterns observed during naturalistic
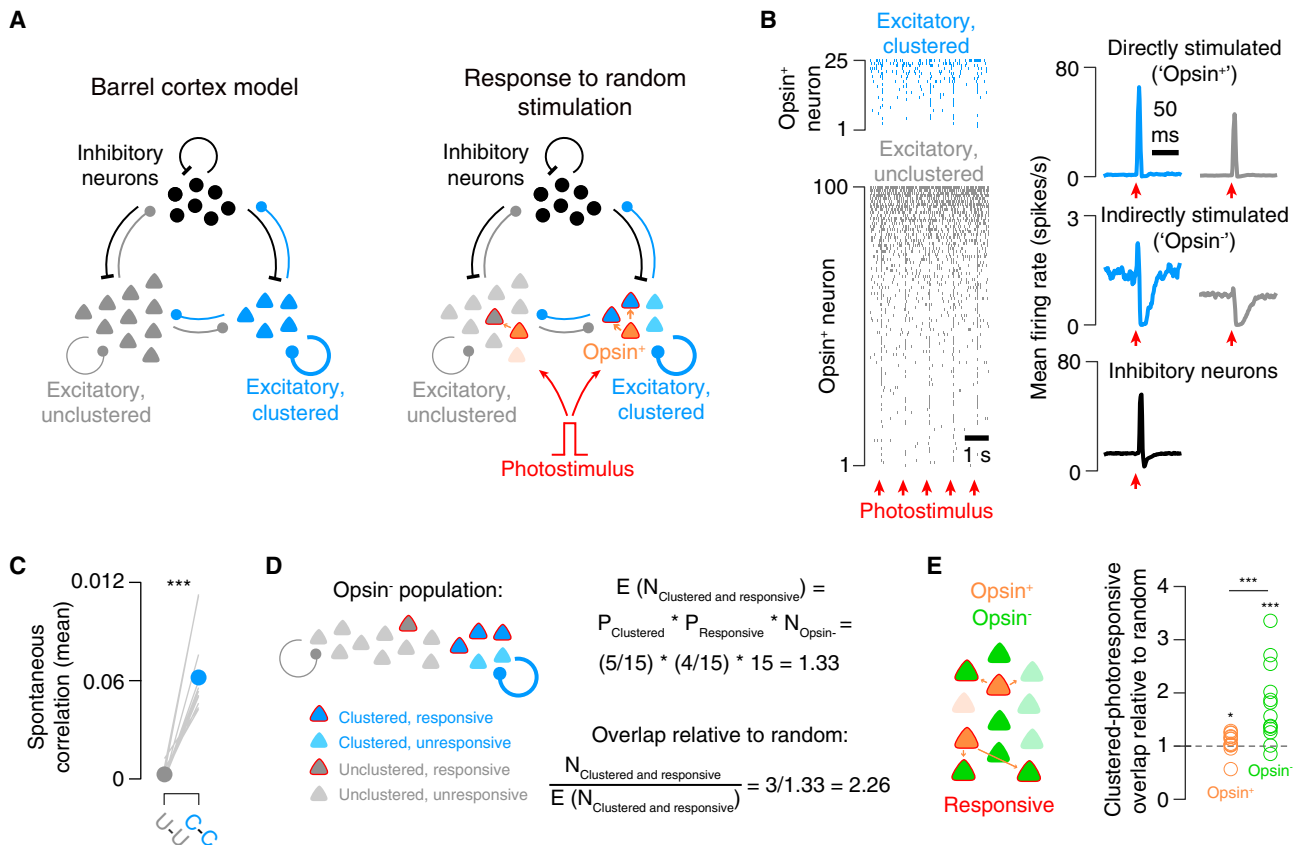
Figure 1. Model of vS1 L2/3 clustered subnetwork response to random stimulation

(A) Integrate-and-fire model of barrel cortex. Left, the model includes 170 clustered excitatory neurons (blue), 1,530 unclustered excitatory neurons (gray), and 300 inhibitory neurons (black). Right, "random" stimulation was simulated by assigning 20% of both clustered and unclustered neurons to the opsin-expressing group (Opsin[+], orange) and stimulating these neurons with a simulated photostimulus (red, 5 ms current pulse). Both neurons that are directly stimulated and indirectly stimulated respond to simulated photostimulation (red outline, darker color).

(B) Example response to simulated photostimulation. Left, raster plots showing response among the top 25 most responsive clustered neurons (blue) and top 100 most responsive unclustered neurons (gray). Right, mean firing rate response among directly (top) and indirectly stimulated (middle) pyramidal neurons (blue, clustered; gray, unclustered) and inhibitory neurons (bottom, black).

(C) Mean pairwise Pearson's correlation of the firing rate during "spontaneous" activity (Methods). Mean correlation among unclustered excitatory neurons (gray) and among excitatory clustered neurons (blue). Each line represents a single network (N = 13). P value across networks for paired Wilcoxon signed rank test. ***, P < 0.001.

(D) Calculation of overlap between the clustered and photoresponsive populations relative to random. Left, composition of the example population (indirectly stimulated, opsin non-expressing population). Right, calculation of overlap relative to random in this simplified example (Methods).

(E) Left, schematic showing propagation of activity from directly stimulated, opsin-expressing (Opsin[+], orange) to indirectly stimulated, opsin non-expressing (Opsin[-], green) neurons. Right, overlap relative to random for opsin-expressing and opsin non-expressing populations. P value within a group is for Wilcoxon signed rank test evaluating whether the median differs from 0.

P value across groups is for paired Wilcoxon signed rank test. ***, P < 0.001; ** P < 0.01.

stimulation and that this biasing can be enhanced through repeated co-presentation of natural and artificial stimuli.

RESULTS

Random stimulation disproportionately recruits neurons with elevated recurrent connectivity in a network model of vS1.

Can random activation of cortex engage pattern completion? To address this, we used an integrate-and-fire model of vS1 layer (L) 2/3[28] in which 170 of 1,700 excitatory neurons exhibited elevated pairwise connectivity (Figure 1A). This

"clustered" subnetwork simulated the touch network in vS1. We randomly assigned 20% (340) of excitatory neurons to be "opsin-expressing." These neurons received a current-based stimulus (5 ms square pulse, 1 Hz) to simulate optogenetic stimulation. Both directly stimulated (opsin-expressing) and indirectly stimulated (opsin non-expressing) neurons in the clustered subnetwork responded more strongly than the comparable populations in the unclustered subnetwork (Figure 1B). Firing rate correlations outside the stimulus epoch ("spontaneous" correlations; see Methods) were higher within the clustered subnetwork (Figure 1C; 0.062 ± 0.022; mean ± S.D.; N = 13 networks) than the unclustered subnetwork

(0.002 ± 0.004; P < 0.001, Wilcoxon signed rank test, paired by network).

To quantify the degree to which clustering increased responsiveness, we computed the overlap between the responsive and clustered populations relative to that expected if responsive neurons were randomly distributed (Figure 1D). For example, for the opsin non-expressing population, we calculated the number of neurons that would be expected to be both clustered and photoresponsive, $E(N_{clustered\ and\ responsive})$, as the product of the probability of being a clustered opsin non-expressing neuron, the probability of being a responsive opsin non-expressing neuron, and the number of opsin non-expressing neurons: $E(N_{clustered\ and\ responsive}) = P_{Clustered} * P_{Responsive} * N_{Opsin-}$. We then counted the number of opsin non-expressing neurons that were both clustered and responsive, dividing this by the expected number to obtain a measure of overlap relative to random. This metric is equal to 1 if the overlap is the same as expected by chance, greater than 1 if overlap is greater than expected, or less than 1 if the overlap is less than expected.

The responsive opsin-expressing population overlapped with the clustered subnetwork more than expected by chance (Figure 1E; overlap relative to random: 1.10 ± 0.18; N = 13 networks, P = 0.027, Wilcoxon signed rank test assessing difference of median from 1). For opsin non-expressing neurons, the overlap was also greater than expected by chance (1.79 ± 0.70, P < 0.001). The overlap for opsin non-expressing neurons was significantly greater than the overlap for the opsin-expressing neurons (P < 0.001, paired Wilcoxon signed rank test). Our model thus shows that neurons belonging to subnetworks with elevated connectivity will be disproportionately engaged by random stimulation. In addition, neurons stimulated indirectly are predicted to show a stronger effect of clustering than those stimulated directly, presumably due to the weaker influence of stimulation on these neurons.

Recording photostimulus-evoked and vibrissal sensory activity in opsin-transfected sensory cortex

We next assessed the relationship between artificially evoked activity and natural sensory responses *in vivo* by measuring responses to direct cortical stimulation or natural vibrissal stimuli. Transgenic mice expressing GCaMP6s in cortical excitatory neurons (Slc17a7-Cre X Ai162)[32] were virally transfected with the soma-restricted opsin ChRmine (AAV-8-CaMKIIa-ChRmine-mScarlet-Kv2.1-WPRE)[25] in layer (L) 2/3 of the primary vibrissal somatosensory cortex (vS1) and implanted with a cranial window (Figure 2A). Mice were trimmed to a single row of whiskers, and the relevant barrel columns were localized using widefield two-photon calcium imaging (Methods; Figure S1). Following the onset of viral expression, opsin was restricted to vS1 and overlapped with the C row barrel columns. The presence of GCaMP in all opsin-expressing neurons confirmed that opsin expression was restricted to excitatory neurons. Animals were trimmed to the two whiskers whose barrel columns most overlapped the opsin-expressing area. A miniature light-emitting diode (LED) was affixed to the cranial window adjacent to the site of opsin expression.

The touch response was assessed in an initial session preceding photostimulation (Methods) by presenting mice with a pole accessible to their spared whiskers. To encourage whisking, mice were given a water reward after pole withdrawal. To assess the response to direct cortical activation, we stimulated the opsin-expressing neurons with the LED (9 pulses, 20 Hz, 5 ms; Figure 2B) in a subsequent session. In both sessions, trials began with a 1s stimulus epoch. This was followed by a short delay period (500 ms), after which an auditory cue signaled mice to lick for a reward during the response epoch (<2 s). Throughout, an intertrial interval of 10–15 s was employed.

We recorded neural activity using volumetric two-photon calcium imaging. In each trial, we imaged neurons across 3 planes (800-by-800 μm, 20 μm axial spacing, one "subvolume") at 7 Hz (Figure 2C). We alternated between two subvolumes every ~100–150 trials. Neurons were separated into opsin-expressing (687 ± 216 neurons per animal; mean ± S.D., N = 13 mice; Table S1) and opsin non-expressing (2,895 ± 540 neurons per animal) based on the presence of mScarlet (Methods). We found photostimulus responsive neurons in both populations, with opsin non-expressing neurons presumably excited by opsin-expressing neurons in a feedforward manner (Figure 2D).

To capture whisker kinematics, we employed high-speed whisker videography (Figure 2E). Whisker position was defined as the azimuthal angle (θ) of the whisker with the face. Tactile input was measured by the touch-induced change in whisker curvature (Δκ), which is proportional to the force acting on the whisker follicle and correlated with the activity of contact-responsive neurons in vS1.[33] We found neurons responsive to both whisker movement (whisking neurons) and object contact (touch neurons; Figure 2F). Thus, both photostimulation and natural vibrissal stimuli evoke robust responses.

Photostimulation and touch-responsive populations overlap more than expected by chance

Does optical microstimulation of sensory cortex disproportionately engage natural sensory representations? To assess this, we compared photostimulation and touch responsiveness across vS1 neurons (Methods). Neurons were considered part of a responsive population (i.e., touch responsive, photoresponsive) if their mean evoked ΔF/F fell into the top 10% of responses following stimulation (Methods). Touch and photostimulation each engaged a distributed population of neurons (Figure 3A), with a subset of neurons responding to both (Figure 3B). Neurons that responded to both stimuli tended to respond less strongly than the neurons most responsive to a given stimulus (Figure 3C). A separate subset of neurons responded to photostimulation and whisking (Figure S2). These neurons also responded less strongly than the neurons most responsive to photostimulation or whisking alone.

We next asked whether the number of neurons responding to both stimuli was greater than, equal to, or less than the number expected by chance. As with the model (Figure 1C), we computed the number of neurons that would be expected to respond to both photostimulation and vibrissal input ("dual-representation" neurons) assuming random draws with replacement from a given population (opsin-expressing or opsin non-expressing; Methods). Dividing the actual number of dual-representation neurons by this expected number, we obtained a measure of overlap relative to random. For touch- and photoresponsive neurons, we measured an overlap relative to random of 1.25 ± 0.40 (N = 13 mice) among opsin-expressing neurons
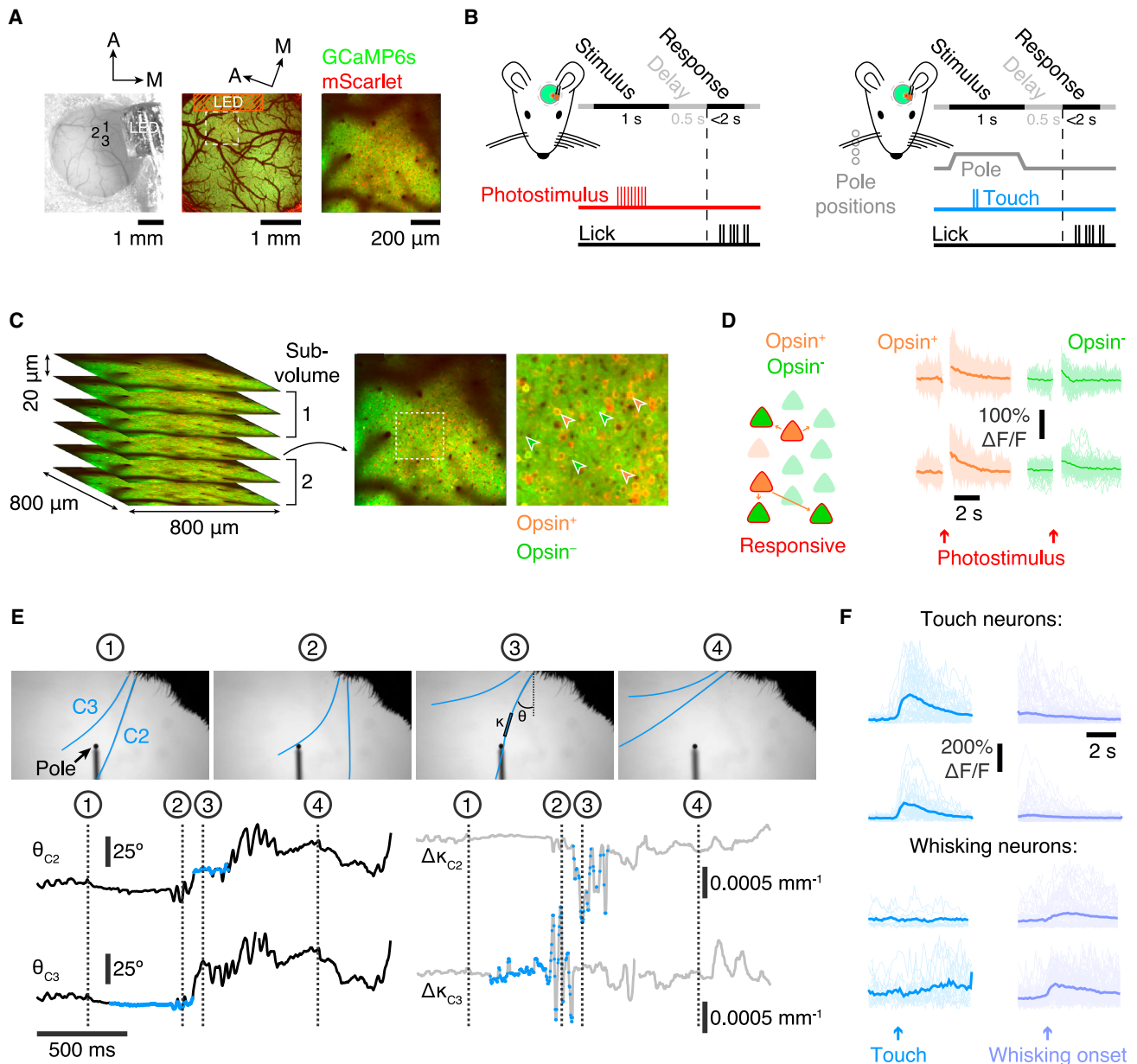
Figure 2. Neurons in L2/3 of vS1 respond to photostimulation, touch, and whisking

(A) Opsin expression in barrel cortex. Left, widefield view of a cranial window showing viral injection sites (numbers) and LED; center, widefield two-photon image of a cranial window after onset of opsin expression (green, GCaMP6s fluorescence; red, mScarlet fluorescence); right, higher magnification two-photon image.

(B) Left, trial structure during a rewarded photostimulation trial. Right, trial structure during a rewarded vibrissal touch trial.

(C) Volumetric two-photon imaging. Subvolumes consist of 3 planes imaged simultaneously at 7 Hz. Left, six planes (800-by-800 μm, 20 μm inter-plane distance, 2 subvolumes); right, example plane with example opsin-expressing (orange) and opsin non-expressing (green) neurons.

(D) Left, schematic showing the expected local propagation of activity from opsin-expressing (orange) to opsin non-expressing (green) neurons. Right, photo-stimulation-evoked $\Delta F/F$ traces for 4 neurons. Light, individual trials; dark, mean. Orange, opsin-expressing; green, opsin non-expressing. A PMT shutter prevented acquisition during photostimulation (Methods).

(E) Whisker videography in an example trial. Top, example frames; bottom, whisker angle (θ, black), and change in whisker curvature ($\Delta\kappa$, gray, see Methods), with touch periods indicated with colored circles.

(F) $\Delta F/F$ traces for 4 neurons aligned to whisker touch (left column) and to whisk onset (right column). Grey, individual trials; black, mean. Top two neurons, touch neurons; bottom two neurons, whisking neurons.
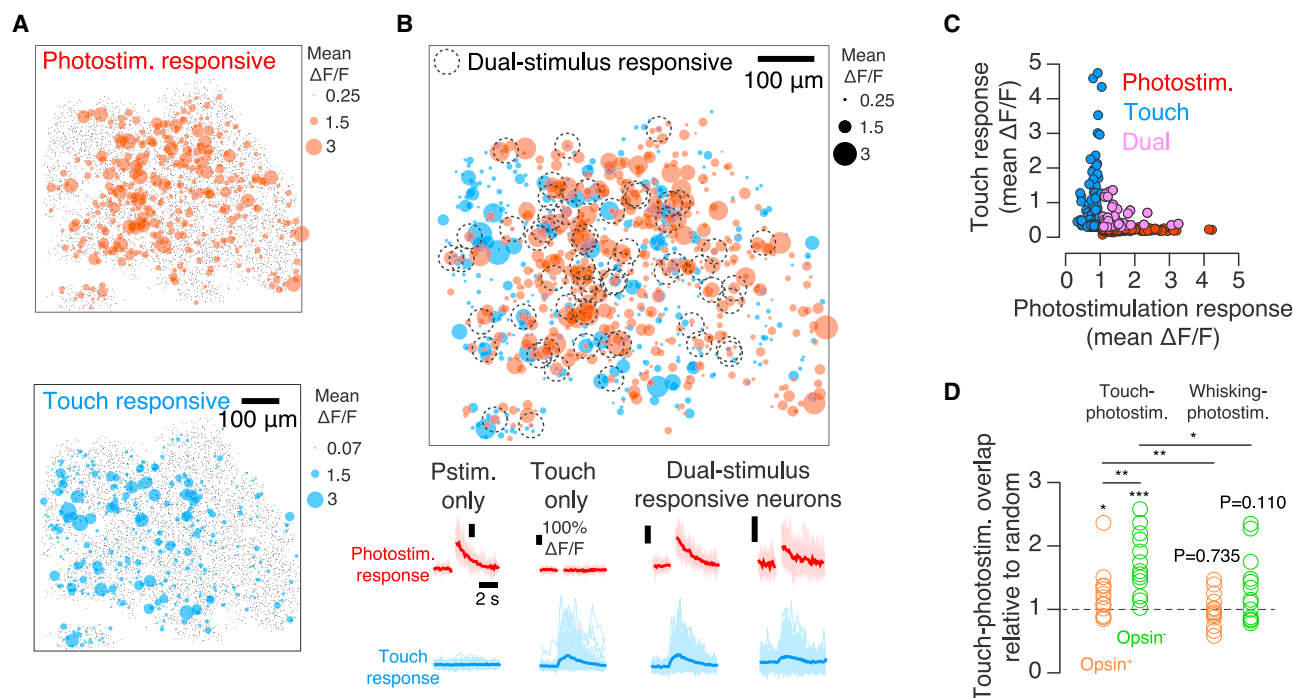
See also Figure S1, Table S1.

Figure 3. Overlap between touch-responsive and photoresponsive populations

(A) Photoresponsive (top, red) and touch-responsive (bottom, blue) populations in an example mouse. Neurons are collapsed across six planes spaced 20 μm apart. Colored circles show the mean touch (blue) or photostimulation (red) evoked ΔF/F across stimulus presentations. Black dots indicate neurons that did not belong to the top 10% of responders (Methods).

(B) Top, overlay of the maps in (A) with non-responsive neurons removed. Neurons belonging to both representations are marked with a black dotted circle. Bottom, stimulus-aligned photostimulation (red, top) and touch (blue, bottom) ΔF/F responses of four example neurons. Dark color, mean response; light color, individual responses.

(C) Relationship between mean ΔF/F touch and photostimulation responses for all responsive neurons in an example mouse (including both opsin-expressing and opsin non-expressing neurons). Blue, neurons that belong only to the top 10% of touch responders; red, neurons that belong only to the top 10% of photostimulation responders; magenta, neurons that belong to both groups (dual).

(D) Overlap between vibrissal- and photostimulation-responsive populations relative to chance for opsin-expressing (orange) and opsin non-expressing (green) neurons across mice (N = 13). P values are given for the Wilcoxon signed rank test assessing whether the median is different than 1 (chance); P values for comparisons between opsin-expressing and opsin non-expressing populations and between touch-photoresponsive and whisking-photoresponsive populations are for the Wilcoxon signed rank test, paired by animal. Left, overlap between touch responsive and photoresponsive population; right, overlap between whisking responsive and photoresponsive population. ***P < 0.001; ** P < 0.01; * P < 0.05.

See also Figures S2, S3 and S4.

(Figure 3D), a value significantly greater than 1 (P = 0.027, Wilcoxon signed rank test assessing whether the median ratio was distinct from 1). Opsin-expressing neurons that respond to optical microstimulation therefore show an elevated likelihood of also being touch responsive.

Our model showed that overlap between the clustered and photoresponsive populations should be greater among opsin non-expressing neurons (Figure 1D), presumably because these neurons are activated indirectly and are therefore more susceptible to intrinsic constraints on response. Consistent with this, the normalized touch-photoresponsive overlap was 1.73 ± 0.48 among opsin non-expressing neurons, which was significantly greater than 1 (P < 0.001) and exceeded the overlap observed in opsin-expressing neurons (P = 0.005, Wilcoxon signed rank test, paired by animal).

Touch but not whisking neurons are recurrently coupled,[28] so if elevated overlap is due to recurrence, whisking neurons should not overlap with photoresponsive neurons more than expected

by chance. For opsin-expressing neurons, we measured a whisking-photoresponsive overlap ratio of 0.99 ± 0.26, a value indistinguishable from 1 (P = 0.735). Whisking-photoresponsive overlap for opsin non-expressing neurons was also indistinguishable from 1 (1.32 ± 0.53; P = 0.110). The touch-photoresponsive overlap ratio differed from the whisking-photoresponsive overlap ratio for both opsin-expressing (P = 0.010, Wilcoxon signed rank test) and opsin non-expressing (P = 0.030) neurons. In sum, whereas the touch responsive population overlapped more than expected by chance with the photoresponsive population, the whisking population did not.

To determine whether opsin expression altered neural physiology, we compared opsin-expressing and opsin non-expressing cells. Opsin-expressing neurons exhibited elevated responses to photostimulation but no differences in touch responsiveness or spontaneous activity levels (Figure S3A). Restricting this analysis to responsive neurons (top 10% of responders to each stimulus; Methods), we found no difference
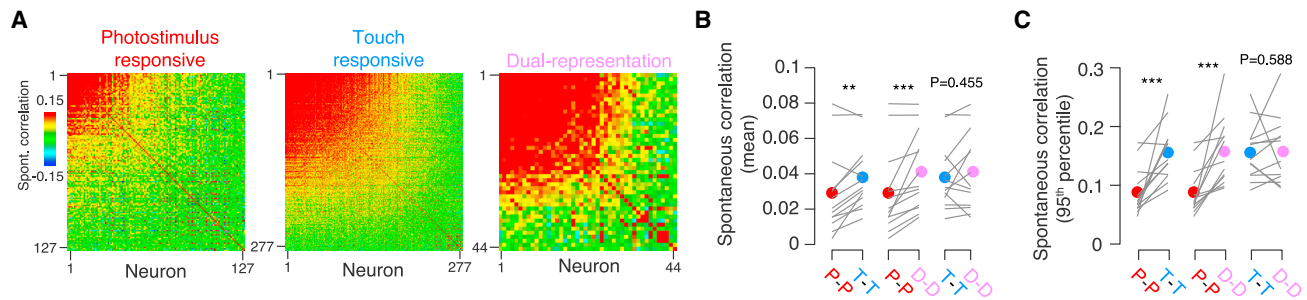
Figure 4. Spontaneous activity correlations within different populations

(A) Pairwise correlations during the inter-stimulus (spontaneous) period in an example mouse. Left, photoresponsive neurons. Middle, touch responsive neurons. Right, dual-representation neurons. Neurons are sorted by their mean correlation to the other neurons within the population.

(B) Mean spontaneous pairwise correlations across mice (N = 13) for photoresponsive (red), touch responsive (blue), and dual-representation (magenta) neurons. P value provided Wilcoxon signed rank test comparing two populations, paired by animal. ***P < 0.001; **P < 0.01; *P < 0.05.

(C) As in (B), but for 95th percentile of spontaneous pairwise correlations.

in any of these properties (Figure S3B). We next examined the neurons with the highest opsin expression, using levels of linearly unmixed mScarlet fluorescence ("redness"; Methods) as a proxy for opsin expression (Figure S4A). Among the top 25% reddest neurons, we again found no difference in any of the examined properties (Figure S3C). Finally, we found levels of opsin expression among touch and whisking neurons comparable to expression levels in the overall population (Figure S3D). We conclude that opsin expression does not alter basic properties of transfected neurons and that transfection is comparably effective among the studied populations.

We next examined how well opsin levels predicted the photostimulation response. The level of opsin expression was correlated with response amplitude among opsin-expressing neurons (Figure S4B). Across animals, this correlation was significantly greater than 0 (Figure S4C; 0.15 ± 0.08; P < 0.001, Wilcoxon signed rank test assessing if the median differs from 0). Thus, opsin expression levels explain some, but not all, of the evoked neural response.

Spontaneous activity correlations are higher among dual-representation neurons

If photostimulation of dual-representation neurons engages recurrence-based pattern completion among touch neurons, spontaneous correlations among neurons with elevated connectivity should be higher, as shown both experimentally[14,15] and in our model (Figure 1C). We therefore examined pairwise correlations within photoresponsive, touch-responsive, and dual-representation populations (Figure 4A), restricting our analysis to "spontaneous" activity during the interstimulus epoch on touch-only imaging sessions (Methods).

Spontaneous pairwise correlations among purely photoresponsive neurons were lower than among purely touch-responsive neurons (photoresponsive: 0.03 ± 0.02; touch: 0.04 ± 0.02, N = 13 mice; P = 0.008, Wilcoxon signed rank test; Figure 4B). Correlations among dual-representation neurons were comparable to the touch population (0.04 ± 0.02; P = 0.455) and greater than correlations among the photoresponsive population (P = 0.001). This effect was especially pronounced among the most-correlated cells: the cross-animal mean of the 95th percentiles of pairwise correlations among photoresponsive neurons

was 0.09 ± 0.04 (Figure 4C) and less than that among touch responsive neurons (0.15 ± 0.05; P = 0.001). Again, dual-representation neurons showed correlations indistinguishable from touch neurons (0.16 ± 0.06; P = 0.588) and substantially greater than photoresponsive neurons (P < 0.001). Thus, neurons responsive to both touch and photostimulation show spontaneous activity correlations comparable to those in touch neurons, whereas neurons responsive only to photostimulation show lower correlations.

Combined touch and photostimulation increases population overlap

Does simultaneous activation of the touch- and photoresponsive populations alter overlap? The plasticity rules governing vS1 L2/3[31] suggest that co-activation of two populations should drive enhanced connectivity due to Hebbian plasticity. We therefore photostimulated opsin-expressing neurons during periods of pole availability (Methods; Figure 5A) over 10 days. A subset of trials featured photostimulation with no pole, allowing us to evaluate the photostimulus-only response, which we did using imaging on the first and final days of this induction protocol. A separate touch-only session (Methods) preceded the first induction session, and another followed the last induction session, allowing us to assess touch responsiveness. Vibrissal kinematics did not differ between pre- and post-induction touch sessions (Figure S5).

Induction increased touch-photoresponsive overlap (Figure 5B). Among opsin non-expressing neurons, overlap increased from 1.76 ± 0.39 to 2.62 ± 1.10 following dual-stimulus induction (Figure 5C; P = 0.016, Wilcoxon signed rank test comparing pre- and post-induction overlap paired by animal; N = 7 mice). This result was robust to the exclusion of any single animal, including the animal with the largest change (increase from 1.68 ± 0.36 to 2.24 ± 0.53; P = 0.031; N = 6 mice). There was no change observed in the opsin-expressing population (pre-induction: 1.26 ± 0.39; post-induction: 1.51 ± 0.65; P = 0.109). Repeated co-presentation of touch and photostimulation therefore resulted in increased representational overlap among opsin nonexpressing neurons.

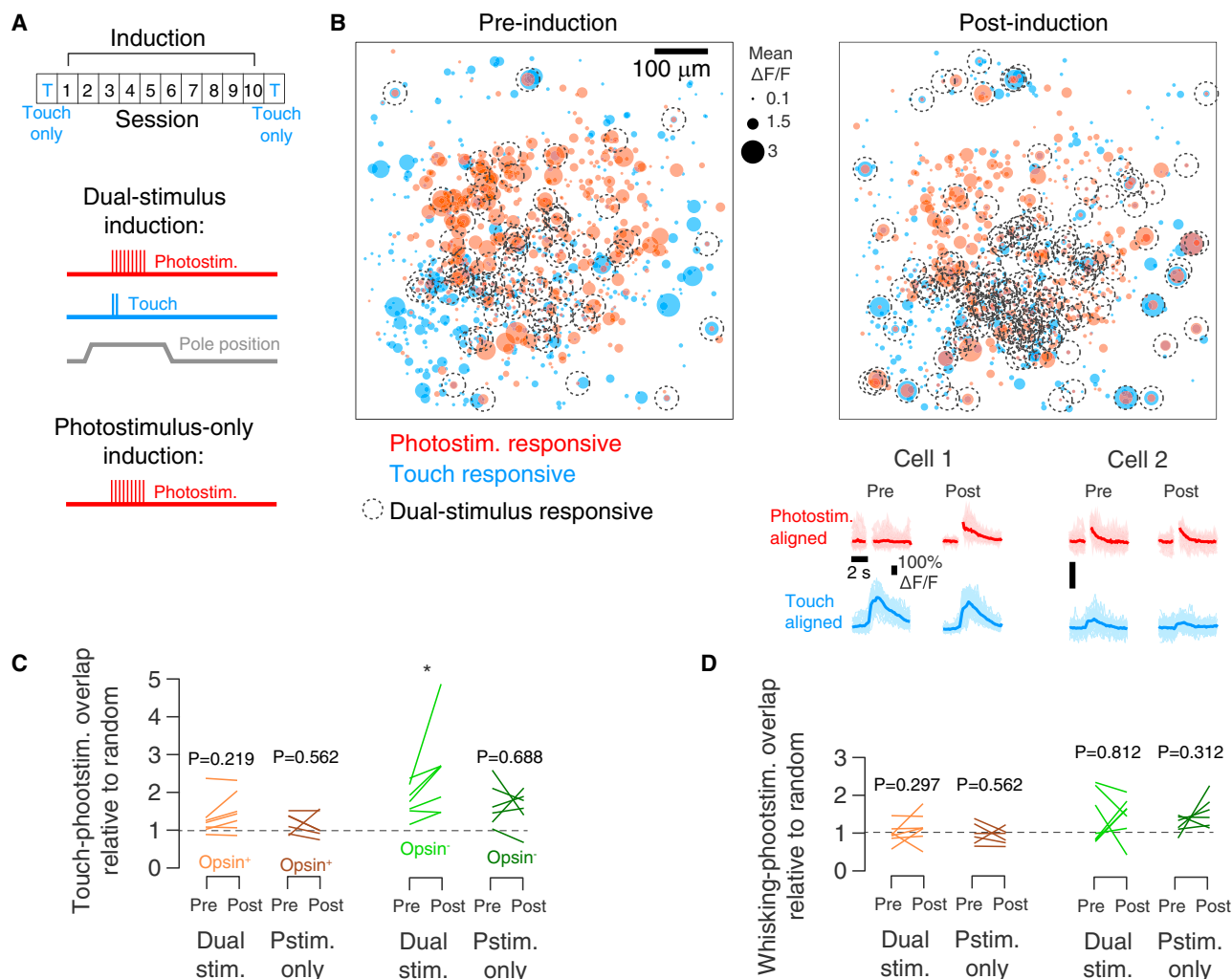In a second group of mice (N = 6), induction consisted of 10 days of optical microstimulation with no touch or reward

Figure 5. Change in overlap between touch and photoresponsive populations following induction

(A) Timeline of the induction experiment. Top, breakdown of sessions in induction experiment. Ten-session induction block is preceded and followed by touch-only sessions (Methods). Middle, dual-stimulus induction features photostimulation (9 pulses; Methods) during the period of pole accessibility. Bottom, photostimulation-only induction does not include pole presentation.

(B) Maps showing the photoresponsive (red) and touch responsive (blue) populations in an example mouse before (left) and after (right) dual-stimulus induction. Colored circles show the mean touch (blue) or photostimulus (red) evoked ΔF/F across stimulus presentations. Neurons belonging to both representations are circled with a dotted line. Bottom, response of two example neurons prior to (left) and after (right) induction.

(C) Touch-photoresponsive overlap among opsin-expressing (orange) and opsin non-expressing (green) populations before and after induction. Mice were exposed to dual-stimulus induction (lighter color, N = 7 mice) or photostimulation-only induction (darker color, N = 6 mice). P values provided for Wilcoxon signed rank test comparing response before and after induction. ***P < 0.001; **P < 0.01; *P < 0.05.

(D) As in (C), but for whisking-photoresponsive overlap.

See also Figures S5, S6.

(Figure 5A). In these animals, overlap did not increase (opsin-expressing overlap: 1.19 ± 0.28 to 1.12 ± 0.34, P = 0.562, N = 6 mice; opsin non-expressing: 1.67 ± 0.58 to 1.57 ± 0.51, P = 0.688). Overlap among whisking and photoresponsive populations did not increase in either population under both induction paradigms (Figure 5D). The change in touch-photoresponsive overlap among opsin non-expressing neurons following dual-stimulus induction (change in overlap: 0.86 ± 0.83, N = 7 mice) was significantly greater than the change in overlap following photostimulation-only induction (−0.09 ± 0.71; P = 0.022, Wilcoxon rank sum test). Thus, dual-stimulus induction

increases overlap between touch- and photoresponsive populations in opsin non-expressing neurons, whereas photostimulation-only induction does not.

We next examined the properties of dual-representation neurons. In contrast to their pre-induction responses, dual-representation neurons had high responses to both photostimulation and touch post-induction (Figure S6A). After dual-stimulus induction, the fraction of opsin-expressing photoresponsive neurons that responded to touch did not change (from 0.13 ± 0.05 to 0.15 ± 0.07; P = 0.375, Wilcoxon signed rank test; Figure S6B). Similarly, no change in the touch-responsive fraction among

photoresponsive neurons was seen in mice exposed to photostimulation-only induction (from 0.11 ± 0.04 to 0.10 ± 0.05, P = 0.562). Among opsin non-expressing neurons in dual-stimulus induction mice, however, the touch-responsive fraction increased from 0.18 ± 0.05 to 0.26 ± 0.11 (P = 0.016); the photostimulation-only condition yielded no change (from 0.17 ± 0.06 to 0.16 ± 0.05, P = 0.688). The fraction of touch neurons that were photoresponsive only changed among opsin non-expressing neurons in dual-stimulus induction mice (from 0.10 ± 0.05 to 0.15 ± 0.05; P = 0.016; Figure S6C). There was no change in this fraction among opsin-expressing neurons (dual-stimulus induction: from 0.31 ± 0.11 to 0.31 ± 0.14, P = 0.938; photostimulation-only induction: from 0.36 ± 0.13 to 0.35 ± 0.21, P = 0.438) or among opsin non-expressing neurons in photostimulation-only induction mice (from 0.07 ± 0.03 to 0.07 ± 0.02, P = 1). In sum, dual-stimulus induction increases the fraction of dual-representation neurons, but only among opsin non-expressing neurons.

We next asked which populations contributed to the post-induction dual-representation population. We restricted our analysis to opsin non-expressing neurons in dual-stimulus induction mice. Of these neurons, 0.21 ± 0.12 (fraction; N = 7 mice) were dual representation prior to induction, 0.24 ± 0.17 were photoresponsive only, 0.20 ± 0.13 were touch responsive only, and 0.21 ± 0.12 did not respond to either stimulus on the first day (Figure S6D). When normalized to the size of the pre-induction populations, previously responsive neurons were more likely than chance to become dual representation: touch neurons were 2.22 ± 1.37 times more likely than chance to become dual representation (P = 0.047, Wilcoxon signed rank test determining if median ratio was equal to 1; Figure S6E), photoresponsive neurons were 5.20 ± 2.95 times more likely than chance to become dual representation (P = 0.016), and dual representation neurons were 22.15 ± 7.29 times more likely than chance to remain dual representation (P = 0.016). Non-responsive neurons were less likely than chance to become dual representation (0.40 ± 0.15; P = 0.016). Neurons that were initially responsive were thus most likely to be dual representation following induction.

Combined touch-photostimulation training sparsens the stimulus response

Did overlap between touch and photoresponsive populations rise because new neurons emerged that were responsive to both stimuli or because induction reduced responsiveness among neurons that did not respond to both stimuli? To assess this, we examined how responsiveness changed following dual-stimulus induction.

Following induction, the responsiveness and membership of both populations changed (Figure 6A). The mean $\Delta F/F$ response to photostimulation among opsin-expressing neurons declined (Figure 6B) from 0.65 ± 0.19 to 0.39 ± 0.10 (N = 7 mice; P = 0.004, Wilcoxon signed rank test, paired by animal). Opsin-expressing neurons in mice exposed to photostimulation alone did not show a change (0.75 ± 0.32 to 0.59 ± 0.25, N = 6 mice; P = 0.394), nor did opsin non-expressing neurons in either induction paradigm (dual-stimulus induction: 0.59 ± 0.25 to 0.43 ± 0.11; P = 0.259; photostimulation-only induction: 0.64 ± 0.20 to 0.51 ± 0.14; P = 0.240). The mean touch

response among opsin-expressing neurons also declined (Figure 6C), from a mean $\Delta F/F$ of 0.19 ± 0.08 to 0.12 ± 0.03 (P = 0.017). Again, opsin-expressing neurons in mice exposed to photostimulation-only induction did not show a significant change in touch response (0.14 ± 0.05 to 0.13 ± 0.02; P = 0.485), nor did opsin non-expressing touch neurons in either induction paradigm (dual-stimulus: 0.20 ± 0.07 to 0.17 ± 0.04; P = 0.456; photostimulation-only: 0.18 ± 0.06 to 0.17 ± 0.02; P = 0.310). We find that both touch and photostimulus responses declined among opsin-expressing neurons in dual-stimulus induction animals.

Stimulus responsiveness for individual members of a sensory cortical representation can change over time in a process known as "representational drift."[34,35] To measure drift, we measured the mean stimulus-evoked $\Delta F/F$ for all neurons of a given mouse pre- and post-induction and computed the Pearson correlation between these two population vectors. The photoresponsive population was more stable than the touch population (Figure 6D). Among animals exposed to dual-stimulus induction (N = 7 mice), the mean correlation between pre- and post-induction photostimulation responses among photoresponsive neurons (Figure 6E; $R_{photostim} = 0.58 \pm 0.13$) was higher than the correlation of touch responses among touch neurons ($R_{touch} = 0.20 \pm 0.15$; P = 0.002, Wilcoxon signed rank test). Photoresponsive populations were more stable than touch populations in opsin-expressing neurons of mice exposed to photostimulus-only induction ($R_{photostim} = 0.79 \pm 0.11$, $R_{touch} = 0.29 \pm 0.22$ P = 0.002) and opsin non-expressing neurons of mice exposed to both dual-stimulus induction ($R_{photostim} = 0.57 \pm 0.20$, $R_{touch} = 0.27 \pm 0.17$; P = 0.026) and photostimulus-only induction ($R_{photostim} = 0.79 \pm 0.11$, $R_{touch} = 0.41 \pm 0.18$; P = 0.002). Thus, photoresponsive populations were more stable than touch responsive populations.

We next examined the impact of induction on whisking-responsive neurons (Figure S7A). In all cases, the aggregate whisking response (mean whisking onset-evoked $\Delta F/F$; Methods) remained unchanged (Figure S7B). As with touch populations, whisking populations exhibited greater drift than photoresponsive populations (Figure S7C and D). Responsiveness declines are thus confined to touch- and photostimulation responsive populations, with photoresponsive neurons exhibiting greater stability than natural vibrissal representations.

Did changes in opsin expression contribute to the changes in responsiveness? Mean redness did not change following induction (Figure S4E and F), implying that opsin levels were stable. Moreover, pre-induction redness could reliably predict post-induction redness, implying that the opsin-expressing population was stable in membership (Figure S4G and H). If opsin levels remained unchanged yet photo-responsiveness declined, this may have been due to a change in the degree to which opsin levels predicted response. Indeed, the correlation between redness and photostimulation-evoked response declined for both types of induction (Figure S4D).

Aggregate responsiveness among both touch- and photoresponsive opsin-expressing neurons thus declines, consistent with dual-stimulus induction engaging homeostatic renormalization of experimentally elevated network activity.[36] Moreover, the photoresponsive population was more stable than the touch-responsive population.
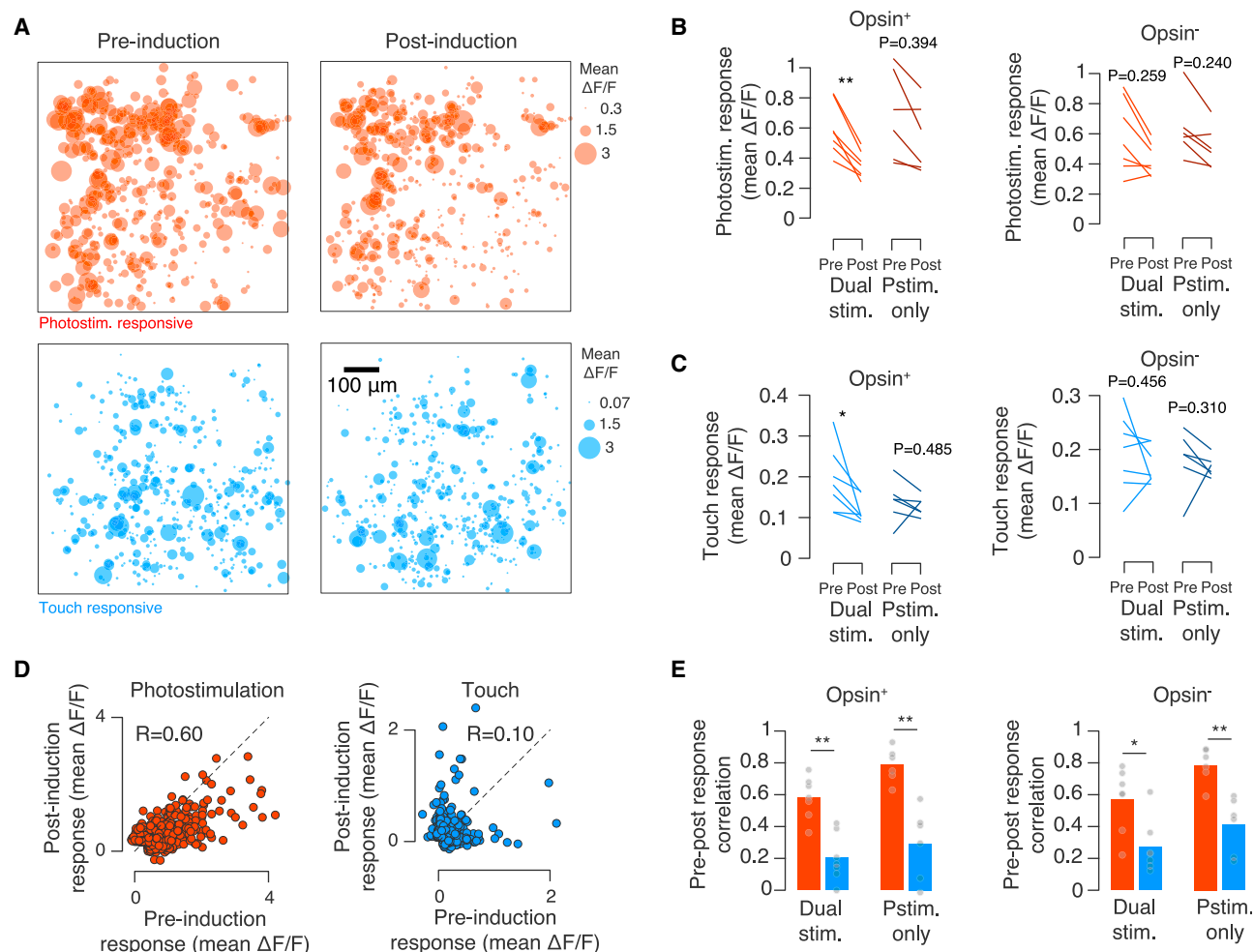
Figure 6. Change in touch and photoresponsive populations following induction

(A) Photoresponsive (top, red) and touch-responsive (bottom, blue) populations in an example mouse before (left) and after (right) dual-stimulus induction. Neurons are collapsed across six imaging planes spaced 20 μm apart. Colored circles show the mean touch (blue) or photostimulation (red) evoked ΔF/F across stimulus presentations.

(B) Change in mean stimulus-evoked ΔF/F among the top 10% of most photoresponsive neurons following induction. Left, opsin-expressing; right, opsin non-expressing. In each case, we examined mice exposed to dual-stimulus induction (N = 7; lighter color), and photostimulation-only induction (N = 6; darker color). P values provided for signed rank test comparing response before and after induction. ***P < 0.001; **P < 0.01; *P < 0.05.

(C) As in (B), but for touch responsiveness.

(D) Stimulus response (mean evoked ΔF/F) before and after dual-stimulus induction. Left (red), photostimulation response among all responsive neurons before and after induction in an example mouse. Right (blue), touch response before and after induction.

(E) Correlation of pre- and post-induction mean evoked ΔF/F for photostimulation responsive (red) and touch responsive (blue) populations. Left, opsin-expressing; right, opsin non-expressing neurons. ***P < 0.001; P < 0.01; *P < 0.05; P value for Wilcoxon signed rank test comparing touch and photoresponsive populations.

See also Figure S7.

Touch-photostimulation training increases spontaneous activity correlations

We next asked if induction altered spontaneous activity correlations, as this would be suggestive of altered connectivity.[14,15] Pairwise correlations during spontaneous activity among photoresponsive neurons increased for both opsin-expressing and opsin non-expressing neurons (Figure 7A). In opsin-expressing neurons, pairwise correlations among photoresponsive neurons increased from 0.02 ± 0.01 to 0.06 ± 0.03 following dual-stimulus induction (P = 0.016, Wilcoxon signed rank test; Figure 7B). Dual-

stimulus induction also increased correlations among photoresponsive opsin non-expressing neurons, from 0.03 ± 0.02 to 0.06 ± 0.02 (P = 0.016). Photostimulation-only induction, however, did not produce a change in correlations among either opsin-expressing (P = 0.688) or opsin non-expressing (P = 0.844) photoresponsive neurons. Thus, dual-stimulus but not photostimulation-only induction increases correlations among photoresponsive neurons.

Did dual-stimulus induction change the correlations between touch and photoresponsive populations? For opsin-expressing
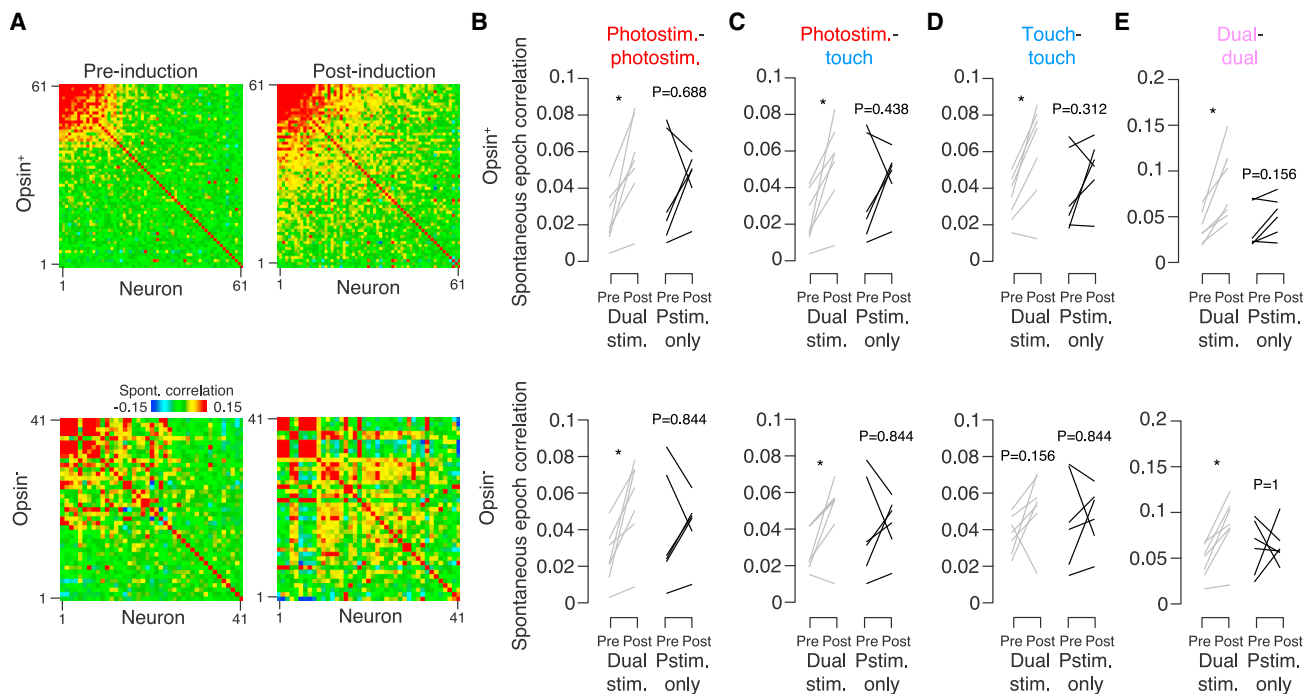
Figure 7. Spontaneous activity correlations before and after induction

(A) Spontaneous pairwise correlation matrices for the photoresponsive population in an example mouse before (left) and after (right) dual-stimulus induction. Top, opsin-expressing population; bottom, opsin non-expressing. Neurons are sorted by their mean correlation to the other neurons within the population.

(B) Mean spontaneous pairwise correlations before and after induction among photoresponsive neurons. Grey, mice that were exposed to dual-stimulus induction (N = 7); black, mice that were exposed to photostimulus-only induction (N = 6). P values provided for Wilcoxon signed rank test comparing fraction before and after induction. P< 0.001; ** P < 0.01; * P < 0.05. Top, opsin-expressing neurons; bottom, opsin non-expressing neurons

(C) As in (B), but for correlations between touch responsive and photoresponsive neurons.

(D) As in (B), but for touch responsive neurons.

(E) As in (B), but for dual-representation neurons.

neurons, dual-stimulus induction increased pairwise correlations between photoresponsive and touch responsive neurons from 0.02 ± 0.02 to 0.05 ± 0.02 (P = 0.016; Figure 7C). Similarly, among opsin non-expressing neurons, dual-stimulus induction increased pairwise correlations between touch and photoresponsive neurons from 0.03 ± 0.01 to 0.05 ± 0.02 (P = 0.016). Photostimulation-only induction did not alter photoresponsive-touch correlations for either opsin-expressing (P = 0.438) or opsin non-expressing (P = 0.844) neurons.

Dual-stimulus induction also increased correlations among opsin-expressing touch neurons, from 0.03 ± 0.01 to 0.06 ± 0.03 (P = 0.031; Figure 7D), though touch-touch correlations remained unchanged among opsin non-expressing neurons (0.04 ± 0.01 to 0.05 ± 0.02, P = 0.156). Photostimulation-only induction did not alter touch-touch correlations among opsin-expressing (P = 0.312) or opsin non-expressing neurons (P = 0.844). Among opsin-expressing dual-representation neurons, correlations increased from 0.04 ± 0.02 to 0.08 ± 0.04 (P = 0.016; Figure 7E), and correlations increased from 0.05 ± 0.02 to 0.09 ± 0.03 among opsin non-expressing neurons (P = 0.016). Photostimulation-only induction again did not alter correlations (opsin-expressing, P = 0.156; opsin non-expressing, P = 1).

Thus, dual-stimulus induction resulted in increased correlations within photoresponsive, touch, and dual-representation

populations, and between photoresponsive and touch responsive populations. Photostimulation-only induction did not alter spontaneous activity correlations.

DISCUSSION

We find that optogenetically stimulating a population of vS1 pyramidal neurons disproportionately engages existing touch but not whisking neurons (Figure 3). Given that touch but not whisking neurons are recurrently coupled,[28] our work suggests that cortical microstimulation may engage recurrent pattern completion.[20] This is consistent with a network model where random photostimulation preferentially engages neurons belonging to a subnetwork with elevated recurrence (Figure 1). This is further supported by our observation that spontaneous pairwise correlations among neurons that are both photoresponsive and touch responsive are comparable to correlations among touch neurons, whereas neurons that are purely photoresponsive show lower pairwise correlations (Figure 4). We also find that repeated co-activation of touch- and photostimulus-responsive neurons increases the number of neurons responding to both stimuli (Figure 5) and enhances spontaneous activity correlations within and between the touch- and photoresponsive populations (Figure 7). Thus, we show that intrinsic network

properties channel artificially introduced cortical activity into patterns observed with natural input and that repeated co-presentation of natural and artificial stimuli enhances this effect.

Will activating a random subset of an area's excitatory neurons produce activity patterns seen with natural sensory input? Cortical activity is typically confined to a small subspace of possible network activity patterns,[1,5,6] potentially due to elevated recurrent connectivity.[2,37] Consistent with this, spontaneous activity resembles evoked activity in the visual,[7,38] auditory, and somatosensory cortices.[8] Moreover, local recurrent connections are highly specific, with small subnetworks of highly and bidirectionally connected neurons embedded in a broader network with lower connectivity.[11,12] These subnetworks likely exhibit similar sensory tuning, as neurons with similar tuning and higher pairwise correlations exhibit higher connectivity.[14,15,39] This suggests that cortical recurrence should favor pattern completion,[20] a prediction borne out in experiments where direct activation of a small number of visual cortical neurons with particular tuning can drive activity in other neurons with similar tuning.[24,25] Our work suggests that even non-specific stimulation of the cortex engages recurrence-mediated pattern completion that, in vS1, results in activation of existing touch- but not whisking-responsive populations. That opsin non-expressing neurons show greater overlap bolsters this conclusion, as opsin non-expressing neurons experience less direct drive from the photostimulus than opsin-expressing neurons and should therefore be more impacted by intrinsic network properties.

Why are so many touch-responsive neurons not photoresponsive and vice-versa? Optogenetic activation of vS1 rapidly engages strong feedback inhibition.[40] Given that opsin-expressing neurons exhibit a range of photosensitivity,[41] it is likely that neurons with weaker or delayed responses are suppressed by such inhibition. That many photoresponsive neurons should not respond to touch is expected, assuming opsin expression is random with respect to touch sensitivity: touch responses in mice with trimmed whiskers are sparse,[26,42] and so the most opsin-expressing neurons are likely to be among the majority that do not respond robustly to touch.

Given the existence of a small subset of L2/3 vS1 neurons that are unusually touch responsive due to higher excitability,[43] it is possible that both natural and artificial excitation engages this subpopulation. In this case, excitability, and not connectivity, could account for the elevated overlap among photoresponsive and touch-responsive populations. Whisking neurons, like touch neurons, are part of the sparse and responsive minority of vS1 pyramidal neurons.[26] However, whisking neurons are not disproportionately engaged via optical microstimulation. Because touch, but not whisking, neurons exhibit recurrent amplification,[28] the lack of elevated overlap with this population argues against excitability as the only explanation. Nevertheless, our experiments do not preclude this as a contributing mechanism, and it is likely that both excitability and connectivity play a role in explaining our results.

What mechanisms drive the reduction in overall response and the increase in touch-photoresponsive population overlap following induction? In slice experiments, repeated optogenetic stimulation drives reduced responsiveness among stimulated neurons and reduced connectivity among stimulated and non-stimulated populations,[44] consistent with a role for both connectivity and excitability. In contrast, repeated stimulation of small[45] and large[46-48] cortical populations in vivo increases responsiveness among the stimulated neurons. Modeling work suggests that whether repeated stimulation alone drives increased or reduced responsiveness depends on coupling between excitatory and inhibitory populations.[49] Our observation of declining overall responsiveness (Figure 6) suggests that our paradigm reduces excitability, similar to results obtained in slice. In addition, our observation of increased overlap and spontaneous pairwise correlations is consistent with elevated connectivity among the stimulated populations. The plasticity rules governing excitatory-excitatory synapses within L2/3 of vS1[31] should yield elevated connectivity under conditions of concurrent touch and photostimulation, as demonstrated in modeling studies.[29,30] Nevertheless, further experiments are needed to determine the precise mechanism driving increased overlap.

The elevated overlap between photoresponsive and touch-responsive populations suggests that even non-specific cortical stimulation may evoke naturalistic touch-like activity patterns and thus, touch sensations. This may explain the effectiveness with which stimulation of somatosensory cortex can perceptually bias animals trained to use natural somatosensory input[21,50] and the long-standing observation that cortical stimulation can evoke both naturalistic percepts[9] and movements.[10] Our work suggests that direct cortical stimulation can evoke naturally occurring patterns of activity without cellular-resolution stimulation. Moreover, our induction experiment suggests that appropriate induction paradigms should enhance the ability of microstimulation to engage naturalistic activity patterns. This suggests that sensory feedback prostheses[51,52] may not require precise stimulation, facilitating their implementation.

In sum, we show that optical microstimulation can engage natural sensory representations. Moreover, repeated co-presentation of photostimulation and natural sensory input increases the degree to which photostimulation engages the natural sensory representation. Our work thus shows that inherent network properties constrain cortical activity and that even untargeted direct cortical stimulation can engage existing natural cortical representations.

STAR★METHODS

Detailed methods are provided in the online version of this paper and include the following:

- KEY RESOURCES TABLE
- RESOURCE AVAILABILITY
  - Lead contact
  - Materials availability
  - Data and code availability
- EXPERIMENTAL MODEL AND SUBJECT DETAILS
  - Mouse lines
- METHOD DETAILS
  - Network model of barrel cortex
  - Surgical preparation
  - Photostimulation system
  - Two-photon microscopy
  - Identification of touch and whisking neurons

- ○ Induction protocols
- ○ Whisker videography and vibrissal representation analysis
- ○ Photoresponsive representation analysis
- ○ Overlap analysis
- ○ Spontaneous activity correlation analysis
- ○ Quantification and statistical analysis

SUPPLEMENTAL INFORMATION

Supplemental information can be found online at https://doi.org/10.1016/j.cub.2023.03.085.

ACKNOWLEDGMENTS

AUTHOR CONTRIBUTIONS

R.P. and S.P. designed the study. R.P. and A.S-Y. carried out all the experiments. R.P. and S.P. performed data analysis and wrote the paper.

DECLARATION OF INTERESTS

The authors declare no competing interests.

REFERENCES

1. Tsodyks, M., Kenet, T., Grinvald, A., and Arieli, A. (1999). Linking spontaneous activity of single cortical neurons and the underlying functional architecture. Science 286, 1943–1946.

2. Okun, M., Steinmetz, N., Cossell, L., Iacaruso, M.F., Ko, H., Bartho, P., Moore, T., Hofer, S.B., Mrsic-Flogel, T.D., Carandini, M., and Harris, K.D. (2015). Diverse coupling of neurons to populations in sensory cortex. Nature 521, 511–515. https://doi.org/10.1038/nature14273.

3. Jazayeri, M., and Afraz, A. (2017). Navigating the Neural Space in Search of the Neural Code. Neuron 93, 1003–1014. https://doi.org/10.1016/j.neuron.2017.02.019.

4. Gallego, J.A., Perich, M.G., Miller, L.E., and Solla, S.A. (2017). Neural Manifolds for the Control of Movement. Neuron 94, 978–984. https://doi.org/10.1016/j.neuron.2017.05.025.

5. Chung, S., and Abbott, L.F. (2021). Neural population geometry: An approach for understanding biological and artificial neural networks. Curr. Opin. Neurobiol. 70, 137–144. https://doi.org/10.1016/j.conb.2021.10.010.

6. Avitan, L., and Stringer, C. (2022). Not so spontaneous: Multi-dimensional representations of behaviors and context in sensory areas. Neuron 110, 3064–3075. https://doi.org/10.1016/j.neuron.2022.06.019.

7. Kenet, T., Bibitchkov, D., Tsodyks, M., Grinvald, A., and Arieli, A. (2003). Spontaneously emerging cortical representations of visual attributes. Nature 425, 954–956. https://doi.org/10.1038/nature02078.

8. Luczak, A., Bartho, P., and Harris, K.D. (2009). Spontaneous events outline the realm of possible sensory responses in neocortical populations. Neuron 62, 413–425.

9. Penfield, W., and Boldrey, E. (1937). Somatic motor and sensory representation in the cerebral cortex of man as studied by electrical stimulation. Brain 60, 389–443.

10. Graziano, M.S.A., Taylor, C.S.R., and Moore, T. (2002). Complex movements evoked by microstimulation of precentral cortex. Neuron 34, 841–851.

11. Song, S., Sjostrom, P.J., Reigl, M., Nelson, S., and Chklovskii, D.B. (2005). Highly nonrandom features of synaptic connectivity in local cortical circuits. PLoS Biol. 3, e68. https://doi.org/10.1371/journal.pbio.0030068.

12. Perin, R., Berger, T.K., and Markram, H. (2011). A synaptic organizing principle for cortical neuronal groups. Proc. Natl. Acad. Sci. USA 108, 5419–5424. https://doi.org/10.1073/pnas.1016051108.

13. Lefort, S., Tomm, C., Floyd Sarria, J.C., and Petersen, C.C.H. (2009). The excitatory neuronal network of the C2 barrel column in mouse primary somatosensory cortex. Neuron 61, 301–316. https://doi.org/10.1016/j.neuron.2008.12.020.

14. Ko, H., Hofer, S.B., Pichler, B., Buchanan, K.A., Sjostrom, P.J., and Mrsic-Flogel, T.D. (2011). Functional specificity of local synaptic connections in neocortical networks. Nature 473, 87–91. https://doi.org/10.1038/nature09880.

15. Cossell, L., Iacaruso, M.F., Muir, D.R., Houlton, R., Sader, E.N., Ko, H., Hofer, S.B., and Mrsic-Flogel, T.D. (2015). Functional organization of excitatory synaptic strength in primary visual cortex. Nature 518, 399–403. https://doi.org/10.1038/nature14182.

16. Wertz, A., Trenholm, S., Yonehara, K., Hillier, D., Raics, Z., Leinweber, M., Szalay, G., Ghanem, A., Keller, G., Rozsa, B., et al. (2015). PRESYNAPTIC NETWORKS. Single-cell-initiated monosynaptic tracing reveals layer-specific cortical network modules. Science 349, 70–74. https://doi.org/10.1126/science.aab1687.

17. Lee, W.C.A., Bonin, V., Reed, M., Graham, B.J., Hood, G., Glattfelder, K., and Reid, R.C. (2016). Anatomy and function of an excitatory network in the visual cortex. Nature 532, 370–374. https://doi.org/10.1038/nature17192.

18. Morgenstern, N.A., Bourg, J., and Petreanu, L. (2016). Multilaminar networks of cortical neurons integrate common inputs from sensory thalamus. Nat. Neurosci. 19, 1034–1040. https://doi.org/10.1038/nn.4339.

19. Yoshimura, Y., Dantzker, J.L.M., and Callaway, E.M. (2005). Excitatory cortical neurons form fine-scale functional networks. Nature 433, 868–873. https://doi.org/10.1038/nature03252.

20. Douglas, R.J., and Martin, K.A.C. (2007). Recurrent neuronal circuits in the neocortex. Curr. Biol. 17. R496–500. https://doi.org/10.1016/j.cub.2007.04.024.

21. Romo, R., Hernandez, A., Zainos, A., and Salinas, E. (1998). Somatosensory discrimination based on cortical microstimulation. Nature 392, 387–390. https://doi.org/10.1038/32891.

22. Salzman, C.D., Britten, K.H., and Newsome, W.T. (1990). Cortical microstimulation influences perceptual judgements of motion direction. Nature 346, 174–177. https://doi.org/10.1038/346174a0.

23. Afraz, S.R., Kiani, R., and Esteky, H. (2006). Microstimulation of inferotemporal cortex influences face categorization. Nature 442, 692–695.

24. Carrillo-Reid, L., Han, S., Yang, W., Akrouh, A., and Yuste, R. (2019). Controlling Visually Guided Behavior by Holographic Recalling of Cortical Ensembles. Cell 178, 447–457.e5. https://doi.org/10.1016/j.cell.2019.05.045.

25. Marshel, J.H., Kim, Y.S., Machado, T.A., Quirin, S., Benson, B., Kadmon, J., Raja, C., Chibukhchyan, A., Ramakrishnan, C., Inoue, M., et al. (2019). Cortical layer-specific critical dynamics triggering perception. Science 365, eaaw5202. https://doi.org/10.1126/science.aaw5202.

26. Peron, S.P., Freeman, J., Iyer, V., Guo, C., and Svoboda, K. (2015). A Cellular Resolution Map of Barrel Cortex Activity during Tactile Behavior. Neuron 86, 783–799. https://doi.org/10.1016/j.neuron.2015.03.027.

27. Peron, S., Chen, T.W., and Svoboda, K. (2015). Comprehensive imaging of cortical networks. Curr. Opin. Neurobiol. 32, 115–123. https://doi.org/10.1016/j.conb.2015.03.016.

28. Peron, S., Pancholi, R., Voelcker, B., Wittenbach, J.D., Olafsdottir, H.F., Freeman, J., and Svoboda, K. (2020). Recurrent interactions in local

cortical circuits. Nature *579*, 256–259. https://doi.org/10.1038/s41586-020-2062-x.

29. Clopath, C., Busing, L., Vasilaki, E., and Gerstner, W. (2010). Connectivity reflects coding: a model of voltage-based STDP with homeostasis. Nat. Neurosci. *13*, 344–352. https://doi.org/10.1038/nn.2479.

30. Litwin-Kumar, A., and Doiron, B. (2014). Formation and maintenance of neuronal assemblies through synaptic plasticity. Nat. Commun. *5*, 5319. https://doi.org/10.1038/ncomms6319.

31. Banerjee, A., Gonzalez-Rueda, A., Sampaio-Baptista, C., Paulsen, O., and Rodriguez-Moreno, A. (2014). Distinct mechanisms of spike timing-dependent LTD at vertical and horizontal inputs onto L2/3 pyramidal neurons in mouse barrel cortex. Physiol. Rep. *2*, e00271, https://doi.org/10.1002/phy2.271.

32. Daigle, T.L., Madisen, L., Hage, T.A., Valley, M.T., Knoblich, U., Larsen, R.S., Takeno, M.M., Huang, L., Gu, H., Larsen, R., et al. (2018). A Suite of Transgenic Driver and Reporter Mouse Lines with Enhanced Brain-Cell-Type Targeting and Functionality. Cell *174*, 465–480.e22. https://doi.org/10.1016/j.cell.2018.06.035.

33. Severson, K.S., Xu, D., Van de Loo, M., Bai, L., Ginty, D.D., and O'Connor, D.H. (2017). Active Touch and Self-Motion Encoding by Merkel Cell-Associated Afferents. Neuron *94*, 666–676.e9. https://doi.org/10.1016/j.neuron.2017.03.045.

34. Marks, T.D., and Goard, M.J. (2021). Stimulus-dependent representational drift in primary visual cortex. Nat. Commun. *12*, 5169. https://doi.org/10.1038/s41467-021-25436-3.

35. Schoonover, C.E., Ohashi, S.N., Axel, R., and Fink, A.J.P. (2021). Representational drift in primary olfactory cortex. Nature *594*, 541–546. https://doi.org/10.1038/s41586-021-03628-7.

36. Gainey, M.A., and Feldman, D.E. (2017). Multiple shared mechanisms for homeostatic plasticity in rodent somatosensory and visual cortex. Philos. Trans. R. Soc. Lond. B Biol. Sci. *372*, 20160157. https://doi.org/10.1098/rstb.2016.0157.

37. Koren, V., and Deneve, S. (2017). Computational Account of Spontaneous Activity as a Signature of Predictive Coding. PLoS Comput. Biol. *13*, e1005355, https://doi.org/10.1371/journal.pcbi.1005355.

38. Berkes, P., Orban, G., Lengyel, M., and Fiser, J. (2011). Spontaneous cortical activity reveals hallmarks of an optimal internal model of the environment. Science *331*, 83–87. https://doi.org/10.1126/science.1195870.

39. Harris, K.D., and Mrsic-Flogel, T.D. (2013). Cortical connectivity and sensory coding. Nature *503*, 51–58. https://doi.org/10.1038/nature12654.

40. Mateo, C., Avermann, M., Gentet, L.J., Zhang, F., Deisseroth, K., and Petersen, C.C.H. (2011). In vivo optogenetic stimulation of neocortical excitatory neurons drives brain-state-dependent inhibition. Curr. Biol. *21*, 1593–1602. https://doi.org/10.1016/j.cub.2011.08.028.

41. Huber, D., Petreanu, L., Ghitani, N., Ranade, S., Hromadka, T., Mainen, Z., and Svoboda, K. (2008). Sparse optical microstimulation in barrel cortex drives learned behaviour in freely moving mice. Nature *451*, 61–64. https://doi.org/10.1038/nature06445.

42. Voelcker, B., Pancholi, R., and Peron, S. (2022). Transformation of primary sensory cortical representations from layer 4 to layer 2. Nat. Commun. *13*, 5484. https://doi.org/10.1038/s41467-022-33249-1.

43. Crochet, S., Poulet, J.F.A., Kremer, Y., and Petersen, C.C.H. (2011). Synaptic mechanisms underlying sparse coding of active touch. Neuron *69*, 1160–1175. https://doi.org/10.1016/j.neuron.2011.02.022.

44. Liu, B., Seay, M.J., and Buonomano, D.V. (2023). Creation of neuronal ensembles and cell-specific homeostatic plasticity through chronic sparse optogenetic stimulation. J. Neurosci. *43*, 82–92. https://doi.org/10.1523/JNEUROSCI.1104-22.2022.

45. Kim, T., Oh, W.C., Choi, J.H., and Kwon, H.B. (2016). Emergence of functional subnetworks in layer 2/3 cortex induced by sequential spikes in vivo. Proc. Natl. Acad. Sci. USA *113*. E1372–1381. https://doi.org/10.1073/pnas.1513410113.

46. Carrillo-Reid, L., Yang, W., Bando, Y., Peterka, D.S., and Yuste, R. (2016). Imprinting and recalling cortical ensembles. Science *353*, 691–694. https://doi.org/10.1126/science.aaf7560.

47. Zhang, D., Yan, X., She, L., Wen, Y., and Poo, M.M. (2020). Global enhancement of cortical excitability following coactivation of large neuronal populations. Proc. Natl. Acad. Sci. USA *117*, 20254–20264. https://doi.org/10.1073/pnas.1914869117.

48. Alejandre-García, T., Kim, S., Pérez-Ortega, J., and Yuste, R. (2020). Intrinsic excitability mechanisms of neuronal ensemble formation. Preprint at bioRxiv. https://doi.org/10.1101/2020.07.29.223966.

49. Sadeh, S., and Clopath, C. (2021). Excitatory-inhibitory balance modulates the formation and dynamics of neuronal assemblies in cortical networks. Sci. Adv. *7*, eabg8411, https://doi.org/10.1126/sciadv.abg8411.

50. O'Connor, D.H., Hires, S.A., Guo, Z.V., Li, N., Yu, J., Sun, Q.Q., Huber, D., and Svoboda, K. (2013). Neural coding during active somatosensation revealed using illusory touch. Nat. Neurosci. *16*, 958–965. https://doi.org/10.1038/nn.3419.

51. Pandarinath, C., and Bensmaia, S.J. (2022). The science and engineering behind sensitized brain-controlled bionic hands. Physiol. Rev. *102*, 551–604. https://doi.org/10.1152/physrev.00034.2020.

52. Tyler, D.J. (2015). Neural interfaces for somatosensory feedback: bringing life to a prosthesis. Curr. Opin. Neurol. *28*, 574–581. https://doi.org/10.1097/WCO.0000000000000266.

53. Brette, R., Rudolph, M., Carnevale, T., Hines, M., Beeman, D., Bower, J.M., Diesmann, M., Morrison, A., Goodman, P.H., Harris, F.C., Jr., et al. (2007). Simulation of networks of spiking neurons: a review of tools and strategies. J. Comput. Neurosci. *23*, 349–398. https://doi.org/10.1007/s10827-007-0038-6.

54. Avermann, M., Tomm, C., Mateo, C., Gerstner, W., and Petersen, C.C.H. (2012). Microcircuits of excitatory and inhibitory neurons in layer 2/3 of mouse barrel cortex. J. Neurophysiol. *107*, 3116–3134. https://doi.org/10.1152/jn.00917.2011.

55. Stimberg, M., Brette, R., and Goodman, D.F. (2019). Brian 2, an intuitive and efficient neural simulator. Elife *8*, e47314. https://doi.org/10.7554/eLife.47314.

56. Chen, T.W., Wardill, T.J., Sun, Y., Pulver, S.R., Renninger, S.L., Baohan, A., Schreiter, E.R., Kerr, R.A., Orger, M.B., Jayaraman, V., et al. (2013). Ultrasensitive fluorescent proteins for imaging neuronal activity. Nature *499*, 295–300. https://doi.org/10.1038/nature12354.

57. Huber, D., Gutnisky, D.A., Peron, S., O'Connor, D.H., Wiegert, J.S., Tian, L., Oertner, T.G., Looger, L.L., and Svoboda, K. (2012). Multiple dynamic representations in the motor cortex during sensorimotor learning. Nature *484*, 473–478. https://doi.org/10.1038/nature11039.

58. Clack, N.G., O'Connor, D.H., Huber, D., Petreanu, L., Hires, A., Peron, S., Svoboda, K., and Myers, E.W. (2012). Automated tracking of whiskers in videos of head fixed rodents. PLoS Comput. Biol. *8*, e1002591, https://doi.org/10.1371/journal.pcbi.1002591.

59. Kleinfeld, D., and Deschenes, M. (2011). Neuronal basis for object location in the vibrissa scanning sensorimotor system. Neuron *72*, 455–468. https://doi.org/10.1016/j.neuron.2011.10.009.

STAR★METHODS

KEY RESOURCES TABLE

REAGENT or RESOURCE	SOURCE	IDENTIFIER
Bacterial and virus strains		
AAV-8-CaMKIIa-ChRmine-mScarlet-Kv2.1-WPRE	Deisseroth Lab	N/A
Experimental models: Organisms/strains		
Transgenic mouse, Ai162	Jackson Labs	JAX 031562
Transgenic mouse, Slc17a7-Cre	Jackson Labs	JAX 023527
Software and algorithms		
Scanimage	Vidrio	
MATLAB	Mathworks	

RESOURCE AVAILABILITY

Lead contact
Further information and requests for resources and reagents should be directed to the lead contact, Simon Peron (speron@nyu.edu).

Materials availability
This study did not generate new unique reagents.

Data and code availability
Source code used in this paper will be made available at http://github.com/peronlab upon publication. Data from this paper will be provided upon reasonable request to the authors.

EXPERIMENTAL MODEL AND SUBJECT DETAILS

Mouse lines
We used adult male (n = 9) and female (n = 4) Ai162 (JAX 031562) X Slc17a7-Cre (JAX X 023527)[32] mice throughout this study (Table S1). These mice express GCaMP6s exclusively in excitatory neurons throughout cortex in a tetracycline transactivator-dependent manner. To suppress expression during development, breeders were fed doxycycline chow (625 mg/kg doxycycline; Teklad), and all pups therefore received doxycycline until weaning. All animal procedures complied with protocols approved by New York University's University Animal Welfare Committee.

METHOD DETAILS

Network model of barrel cortex
We modeled the L2/3 network associated with a single barrel column as described previously.[28] The network was composed of 2,000 leaky integrate and fire neurons.[53] The dynamics of each neuron were governed by:

$$\tau \frac{dV_i}{dt} = V_r - V(t) + R\left[I_i^{\text{exc}}(t) + I_i^{\text{inh}}(t) + O_i I_i^{\text{ext}}(t)\right]$$

where V is the membrane potential, V_r is the rest/reset potential, τ is the membrane time constant, R is the input resistance, I^{exc} is the excitatory synaptic current, I^{inh} is the inhibitory synaptic current, O is the fractional opsin expression, I^{ext} is the current generated by the sensory stimulus (i.e., the photostimulus), and i indexes the neurons in the network. The synaptic currents follow kick-and-decay dynamics governed by:

$$\tau_{\text{syn}} \frac{dI_i^{\text{syn}}}{dt} = -I_i^{\text{syn}} + \tau_{\text{syn}} \sum_{j,k} w_{ij} \delta(t - t_i^{\text{syn}} - t_d)$$

where "syn" denotes the type of synapse (excitatory or inhibitory), τ_{syn} is the synaptic time constant, w_{ij} is a matrix of synaptic weights from neuron j to neuron i, t_{jk} is the time of the kth spike of neuron j, and t_d is the spike transmission delay. Membrane and synaptic time constants, the refractory period length, and the spike transmission delay were assigned based on experimental measurements in L2/3 of barrel cortex.[13,28,54]

Within the network, 1,700 neurons (85%) were excitatory and 300 (15%) were inhibitory. The excitatory population was further divided into two groups: a clustered subnetwork of 170 neurons (10% of the excitatory population) and an unclustered subnetwork of 1,530 neurons (the remaining 90% of the excitatory population). Therefore, each neuron belonged to one of three groups: the clustered excitatory subnetwork (C), the unclustered excitatory subnetwork (U), or the inhibitory population (I). The clustered subnetwork was used to emulate recurrently coupled touch neurons in barrel cortex.[28] The connection probability (P) between neurons in this subnetwork was therefore elevated ($P_{CC} = 0.4$) compared to the connection probability between neurons in the unclustered subnetwork ($P_{UU} = 0.2$). We used sparse connectivity between the excitatory subnetworks ($P_{CU} = P_{UC} = 0.2$) and dense connectivity both within the inhibitory population as well as between the excitatory and inhibitory populations ($P_{II} = P_{CI} = P_{UI} = P_{IC} = P_{IU} = 0.6$).

The stimulus drive to the network was modeled as an external current targeting a population of 'opsin-expressing' neurons in the excitatory population. A random subset (20%) of excitatory neurons drawn without consideration for clustering were assigned to the opsin-expressing population. The fractional level of opsin expression O for opsin-expressing neurons drawn from a uniform distribution between 0 and 1, resulting in a range of stimulus responsiveness among the 'opsin-expressing' neurons. For each stimulus presentation, the current waveform I^{ext} was modeled as a square pulse (5 ms duration). The peak amplitude of the stimulus waveform was chosen so that the number of responsive neurons was close to that observed experimentally with optical microstimulation. Neurons were stimulated with an amplitude that was proportional to O. Neurons also received tonic background input in the form of a Poisson spike train of excitatory spikes with a frequency of 2,250 Hz for excitatory neurons and 3,050 Hz for inhibitory neurons. These values were selected to maintain a tonic firing rate for each population while preventing runaway excitation. Stimulation was applied at 1 Hz over the course of a 20 s simulation.

Simulations were performed in Python using the the Brian2 simulation package[55] with a step-size of $dt = 0.1$ ms. For each simulation (N = 13), we randomized the opsin-expression and network connectivity. We simulated for 20 s of model time, corresponding to 20 stimulus presentations, and recorded spike trains for all neurons. Firing rate was computed using 1 ms bins. The stimulus-evoked response was then computed by taking the mean firing rate during each stimulus presentation and subtracting the mean firing rate in the 100 ms prior to that stimulus presentation. The 10% of excitatory neurons (170 neurons) with the largest stimulus-evoked response were defined as responsive to photostimulation. Photoresponsive neurons were then partitioned into opsin-expressing and opsin non-expressing neurons. Across simulations, photoresponsive neurons were predominantly opsin-expressing (83.1%). Pairwise 'spontaneous' firing rate correlations were computed using 10 ms bins due to the low firing rate in the interstimulus epoch. Correlation calculations exclude the time window starting 10 ms prior to simulated photostimulus onset and ending 20 ms after onset.

Surgical preparation

Mice (6-9 weeks old) were anesthetized with isoflurane during viral injections, window implantation, LED placement, and whisker trimming (3% induction, 1.4% maintenance). During surgery, a titanium headbar was affixed to the skull with cyanoacrylate (Vetbond). A circular craniotomy (3.5 mm diameter) was then drilled over left vs.1 (center: 3.3 mm lateral, 1.7 mm posterior from bregma) using a dental drill (Midwest Tradition, FG 1/4 drill bit).

Following removal of the bone flap, a viral vector encoding the soma-localized opsin ChRmine and the red fluorophore mScarlet (AAV-8-CaMKIIa-ChRmine-mScarlet-Kv2.1-WPRE, 2.48×10^{13} vg/mL, diluted either 1:200 or 1:500 in 1X PBS; generously provided by Karl Deisseroth) was injected into vs.1. A glass capillary (Wiretrol II, Drummond) was pulled to have a tip diameter of 25 μm using a micropipette puller (P-97, Sutter Instrument) and then beveled to a 30° tip. The pipette was back-filled with mineral oil (M5904, Sigma-Aldrich) and 2 μL of viral solution drawn into the tip using a plunger. One, 20 nL injection or three, 100 nL injections were made 250 μm below the dura (Table S1). When performing multiple injections, injections were spaced 400 μm apart in a triangle centered on the craniotomy. For each injection: (1) the pipette was lowered into the brain at a rate of 300 μm/min, (2) there was a 1-minute pause, (3) virus was injected at a rate of 20 nL/min using a hydraulic micromanipulator (Narishige MO-10), (4) there was a 2 min pause, and (5) the pipette was withdrawn at a rate of 300 μm/min with (6) an additional 1 min pause at a depth of 125 μm below the dura. Following injections, the dura was removed using a pair of fine forceps (Fine Science Tools). A double-layer cranial window (4.5 mm external diameter, 3.5 mm inner diameter; #1.5 coverslip; adhered with Norland 61 UV glue) was then placed over the craniotomy and the skull covered with dental acrylic (Orthojet, Lang Dental) to affix the cranial window and headbar. Mice were post-operatively injected with 1 mg/kg of buprenorphine SR and 5 mg/kg of ketoprofen.

Following surgical recovery, mice were trimmed to whiskers C1-3 and placed on water restriction. To confirm that the area of opsin-expression fell within vs.1, the location of the C1-3 barrel columns was identified (Figures S1A-C). Mice were first head fixed and neural activity throughout the cranial window observed at coarse resolution (4X objective; 3 × 3 mm field of view). A pole was brought into the whisking plane and moved in a posterior direction (1-2 mm) so as to touch each whisker individually. The touch-evoked ΔF/F was used to localize the whisker barrel column.

Following barrel identification and identification of the opsin-expressing region, the photostimulation LED was placed. LEDs (590 nm, LXZ1-PL01, Lumileds) were fabricated by soldering 3 cm of polyurethane enameled copper wire (34 AWG) to each pad of the LED. A 2-pin, flat flex cable connector (Digikey) was soldered to the free ends of the copper wire and secured with epoxy (Devcon). The LED was waterproofed using a thin layer of clear nail polish (Sally Hansen). LEDs were affixed to the animals' cranial

windows under anesthesia. The anterior medial edge of the craniotomy was exposed by drilling away a 60° arc of dental cement and covering the drilled area with cyanoacrylate. Electrical tape was placed over the headbar to prevent current from passing between the LED wires and the headbar. The LED was placed over the drilled area 0.5–1 mm away from the site of opsin expression and at a 30° angle relative to the plane of the window (Figure 2A); LEDs placed further than 1 mm away typically failed to evoke responses. The LED and copper wires were secured to the dental cement using cyanoacrylate, and the LED connector was secured to the posterior edge of the headbar in a similar manner. Waterproofing was confirmed by placing water on the cranial window and ensuring that no current passed between the water and the LED.

Photostimulation system

Optogenetic stimulus delivery was controlled by a LabJack T7 driven by a Raspberry Pi. Stimulus voltage waveforms were generated using custom MATLAB software on a separate computer and sent to the Raspberry Pi. The Raspberry Pi loaded waveforms onto the LabJack and waited for a stimulus trigger. Upon receipt of the trigger, the waveforms were sent to the stimulation and masking flash LED drivers (T-cube, ThorLabs) and the PMT shutters. The signal to the stimulation LED was terminated using a 4-pin, flat flex cable connector (Digikey) that could be mated to the LED connector when the animal was head-fixed. The masking flash consisted of 3 LEDs (595 nm, XPEBAM-L1-0000-00A01, Cree LED) that were spectrally matched to the stimulation LED and placed around the animal's face to illuminate the eyes.

Two-photon microscopy

Calcium imaging was performed using a custom two-photon microscope (http://openwiki.janelia.org/wiki/display/shareddesigns/MIMMS). The microscope consisted of a 940 nm laser (Chameleon Ultra 2, Coherent), a Pockels cell (350-80-02, Conoptics), two galvanometer scanners (6SD11268, Cambridge Technology), a resonant scanner (6SC08KA040-02Y, Cambridge Technology), a 16x objective (N16XLWD-PF, Nikon), an emission filter for green fluorescence (FF01-510/84-30, Semrock), an emission filter for red fluorescence (FF01-650/60, Semrock), and two GaAsP PMTs (H10770PB-40, Hamamatsu) and two PMT shutters (VS.14S1T1, Vincent Associates).

Imaging data was acquired using Scanimage (Vidrio Technologies). Three 800-by-800 μm imaging planes axially spaced 20 μm apart were acquired at a rate of ∼7 Hz (one subvolume). Two adjacent subvolumes were acquired for each animal and alternated every ∼100-150 trials. The objective was moved axially with a piezo (P-725KHDS, Physik Instrumente). Power was depth-adjusted by the acquisition software with an exponential length constant of ∼250 μm.

Imaging data were processed on the NYU High Performance Computing cluster using a semi-automated software pipeline.[26] The pipeline performs image registration, segmentation, neuropil subtraction, ΔF/F computation, and calcium event detection. Segmentation was performed in a semi-automatic fashion for each imaging plane. First, a reference imaging session was selected from all imaging sessions. Using the mean image across the session from the green (GCaMP6s) channel, template convolution using annular and elliptical masks was first used to identify putative neuronal centers. These centers were then passed through an annulus detection algorithm that assigns pixels to specific neurons.[56] Finally, the algorithmically-derived neurons were manually curated. For non-reference sessions, normalized cross-correlation was used to generate a mapping from the reference session mean image to the target session, as described previously.[57]

Opsin expression was measured using mScarlet fluorescence collected in the red PMT channel. For each pixel, we calculated a 'redness score', which consisted of the red channel pixel value following linear unmixing to remove cross-talk introduced by GCaMP fluorescence (Figure S4A). For each neuron, an overall redness score was found by computing the mean unmixed redness across its pixels. For each mouse, we manually selected a value above which neurons were considered opsin-expressing. Neurons with a redness below a second, lower threshold were considered opsin non-expressing. Neurons with an intermediate redness were considered ambiguous and were excluded from population-specific analyses.

Identification of touch and whisking neurons

An imaging session was used to assess touch and whisking sensitivity prior to the first induction session and after the final induction session (Figure 5A). The first touch session occurred in animals never exposed to optogenetic stimulation. During touch sessions, a 0.5 mm diameter pole was brought into the whisking plane for 1 s (Figure 2B). To encourage whisking, mice were rewarded with water following a 0.5 s delay period. Water was delivered from a single lickport if mice licked within 2 s of the end of the delay period ('response' epoch). Mice were given a fixed amount of time (1-2 s) to collect water upon responding. Trials lasted 10-12 s, with variability resulting from when the response occurred during the response epoch. High-speed whisker videography was used to track whiskers throughout the imaging session and classify neurons as either touch- or whisking-responsive (see below).

Induction protocols

Animals were presented with one of two induction protocols: either photostimulus-only or dual photostimulus and touch (Table S1). For mice exposed to the photostimulation-only induction protocol, mice were presented with 9 pulses (5 ms duration, 20 Hz frequency) from the photostimulation LED on 50% of trials. During the photostimulation epoch, the PMT shutters were closed and the masking flash LED was illuminated (9 pulses, 15 ms duration, 20 Hz frequency, pulses centered on the photostimulation LED pulses). On the remaining 50% of trials, no stimulus was presented but the masking flash and PMT shutters were still activated. This allowed us to assess whether neurons were visually responsive or responsive to the auditory cue produced by the shutter. Trials

proceeded with an interstimulus interval of 10 s. Mice were presented with 453.1 ± 33.2 trials per session for 10 sessions. Photostimulation trials in the first photostimulus-only induction session were used to assess for overlap prior to induction (Figure 2).

For mice exposed to dual photostimulus and touch induction, four trial types were used. On 50% of trials, no stimulus was presented but the masking flash and PMT shutters were activated. This allowed us to assess whether neurons were visually responsive or responsive to the auditory cue produced by the shutter. On 16.67% of trials, only a photostimulus was presented; on another 16.67% of trials, only a pole stimulus was presented; on the remaining 16.67% of trials, both stimuli were presented (Figure 5A). Mice were presented with 387.1 ± 54.8 trials per session for 10 sessions. In the dual-stimulus induction mice, to encourage whisking, mice were given a water reward for licking the right of two lickports on trials when a stimulus was present, and the left of two lickports when stimuli were absent. Stimulus presentation and response were separated by a 0.5 s delay. Photostimulus-only trials in the first dual-induction session were used to assess for overlap prior to induction (Figure 2).

Whisker videography and vibrissal representation analysis

Mice were trimmed to the C1-2 or C2-3 whiskers (Table S1) prior to the pre-induction touch and whisking sensitivity assessment and regularly trimmed over subsequent days. Whisker video was acquired from a CMOS camera (Ace-Python 500, Basler) running at 400 Hz and 640 x 352 pixels with a telecentric lens (TitanTL, Edmund Optics). A pulsed 940 nm LED (SL162, Advanced Illumination) was used to illuminate the camera's field-of-view (typical exposure and illumination duration: 200 μs). Custom MATLAB software was used to control video acquisition. 7 s of each trial were recorded, including 1s prior to pole movement, the period when the pole was in reach, and several seconds after the pole was retracted.

Whisker video was processed on NYU's High Performance Computing (HPC) cluster. Candidate whiskers were first detected using the Janelia Whisker Tracker.[58] Whisker identity was then refined and assessed across a single session using custom MATLAB software.[26,28] Following whisker assignment, whisker curvature (κ) and angle (θ) were calculated at specific locations along the whisker's length. Whisking setpoint, amplitude, and velocity were computed by decomposing the whisker angle (θ) using the Hilbert transform.[59] Whisker bout onset was defined as the point where the whisking amplitude reached at least 10°. Change in curvature, Δκ, was calculated relative to a baseline, angle-dependent curvature value obtained during periods when the pole was out of reach. Following automatic touch detection, touch assignment was manually curated using a custom MATLAB user interface.[26] As per convention, protractions were assigned negative Δκ values.

Neurons were assigned to the touch or whisking representations based on the evoked ΔF/F response following touch or whisking bout onset. First, a baseline ΔF/F was computed for each neuron by taking the mean ΔF/F over the 5.5 s prior to each touch or whisking bout onset. Then, a response ΔF/F was computed by taking the mean ΔF/F over the 2 s following touch or whisking bout onset. The evoked ΔF/F was the difference between the response and control ΔF/F. The mean evoked ΔF/F was then computed across trials for each neuron. Neurons were considered to be 'whisking' neurons if their mean evoked ΔF/F fell into the top 10% of neurons following whisking bout onset. Similarly, neurons were considered 'touch' neurons if their mean evoked ΔF/F fell into the top 10% of neurons following touch onset. This cut-off is in line with estimates of the percentage of touch (17%) and whisking (17%) L2/3 excitatory neurons in the whisker barrel column (Peron et al. 2015).

Photoresponsive representation analysis

Neurons were classified as responsive or non-responsive by computing the photostimulation-evoked ΔF/F. A baseline ΔF/F was computed for each neuron by taking the mean of the ∼5.5 s (39 frames) preceding shutter closure on each trial. The post-stimulation ΔF/F was calculated as the mean ΔF/F of the two frames immediately following shutter reopening. For each trial, the photostimulation-evoked ΔF/F was found by taking the difference between the post-stimulation ΔF/F and the baseline ΔF/F. Neurons were considered photoresponsive in any given session if they fell within the top 10% of neurons based on the mean photostimulation-evoked ΔF/F computed across photostimulation trials.

Overlap analysis

For any two representations A and B, we computed the expected number of neurons belonging to both representations assuming they were randomly related, where is the number of neurons in the sub-population in question (opsin-expressing or opsin non-expressing). Both and were calculated for a given subpopulation (opsin-expressing or opsin non-expressing). For instance, to calculate overlap between touch and photoresponsive neurons, we used the aforementioned 10% criteria applied to all neurons to determine which neurons were touch and photoresponsive. We then examined opsin-expressing and opsin non-expressing populations separately. Though touch and whisking neurons were not discernibly different in frequency for opsin-expressing and opsin non-expressing populations (Figure S3), photoresponsive neurons were more concentrated among the opsin-expressing populations.

To calculate the overlap between A and B relative to random, , we divided the actual number of neurons in both representations by this number:. A two-tailed Wilcoxon signed rank test was used to test the null hypothesis that the median value of = 1. Upon rejection of the null hypothesis, implies that there are fewer neurons belonging to both representations than expected by chance, whereas implies an overlap larger than expected by chance. In our data, we only observed significant values greater than one. For overlap prior to induction (Figure 3D, 5C, 5D), we used the first touch only session and the first photostimulation session; overlap prior following induction (Figures 5C and 5D), we used the final touch only session and the final photostimulation session.

Spontaneous activity correlation analysis

To compute pairwise correlations between neurons during non-stimulus epochs, we restricted our analysis to the touch-only sessions. We sampled from the time period 5 s after the pole stimulus was removed and computed correlations between ΔF/F vectors for all pairs of simultaneously imaged neurons.

Quantification and statistical analysis

For comparisons between paired samples, we used the Wilcoxon signed rank test. For unpaired samples, we used the Wilcoxon rank sum test. For correlation tests, Pearson's correlation was used to identify a linear correlation coefficient (R) and test for significance.

Supplemental Information

Microstimulation of sensory cortex

engages natural sensory representations

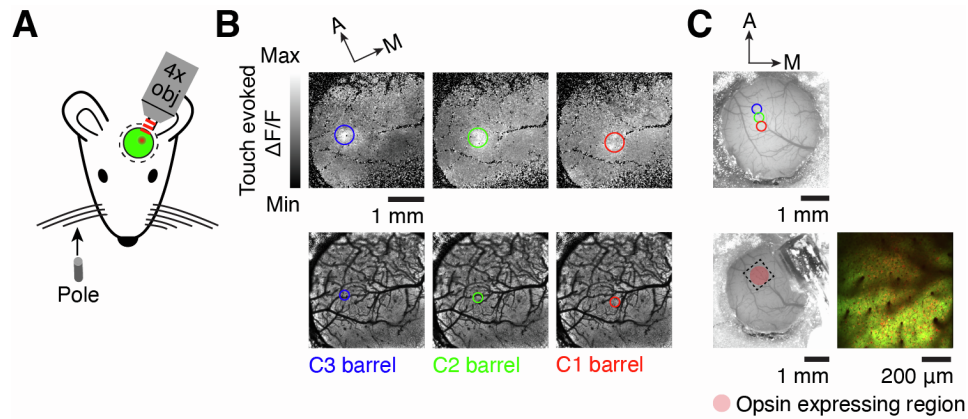Ravi Pancholi, Andrew Sun-Yan, and Simon Peron

Figure S1. Targeting single barrel for superficial opsin expression, related to Figure 2.

(A) Barrel mapping was conducted by moving a pole toward the C1, C2, or C3 whiskers during widefield (4x) two-photon calcium imaging.

(B) Touch-evoked ΔF/F following whisker stimulation. ΔF/F after touch by indicated whisker (top) and barrel column locations on corresponding vasculature (bottom).

(C) Cranial window before (top) and after (bottom) LED placement. Higher magnification two-photon image of opsin-expressing area (right). Colored circles indicate the identified barrel locations from (B), and the dotted circle indicates the site of opsin expression.
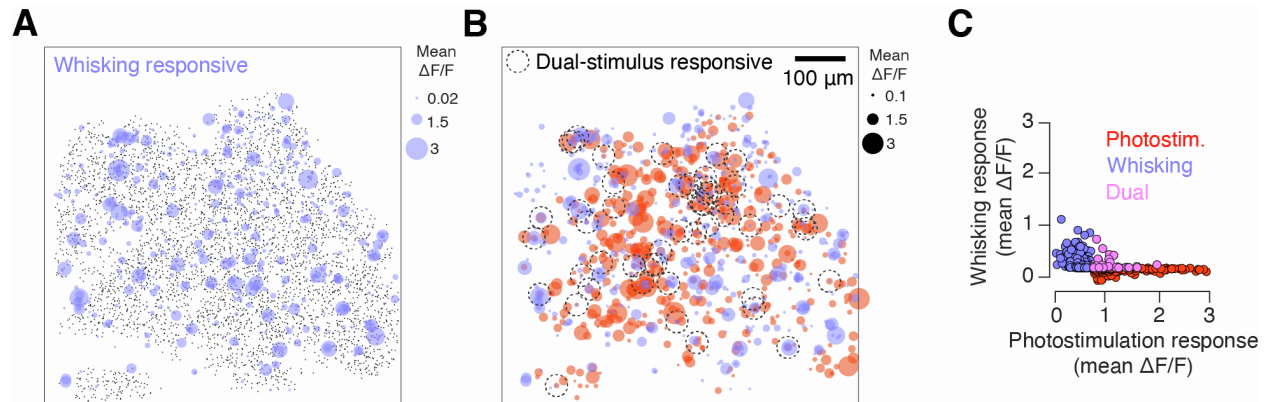
Figure S2. Overlap between whisking and photoresponsive populations, related to Figure 3.

(A) Whisking population in an example mouse (same as in **Figure 3**). Neurons are collapsed across six planes spaced 20 μm apart. Colored circles show the mean whisking evoked ΔF/F across stimulus presentations. Black dots indicate neurons that did not belong to the top 10% of responders (Methods).

(B) Overlay of the whisking and photoresponsive maps, with non-responsive neurons removed. Neurons belonging to both representations are marked with a black dotted circle.

(C) Relationship between mean ΔF/F whisking and photostimulation responses for all responsive neurons in an example mouse (including both opsin-expressing and opsin non-expressing neurons). Purple, neurons that belong only to the top 10% of whisking responders; red, neurons that belong only to the top 10% of photostimulation responders; magenta, neurons that belong to both groups ('dual').
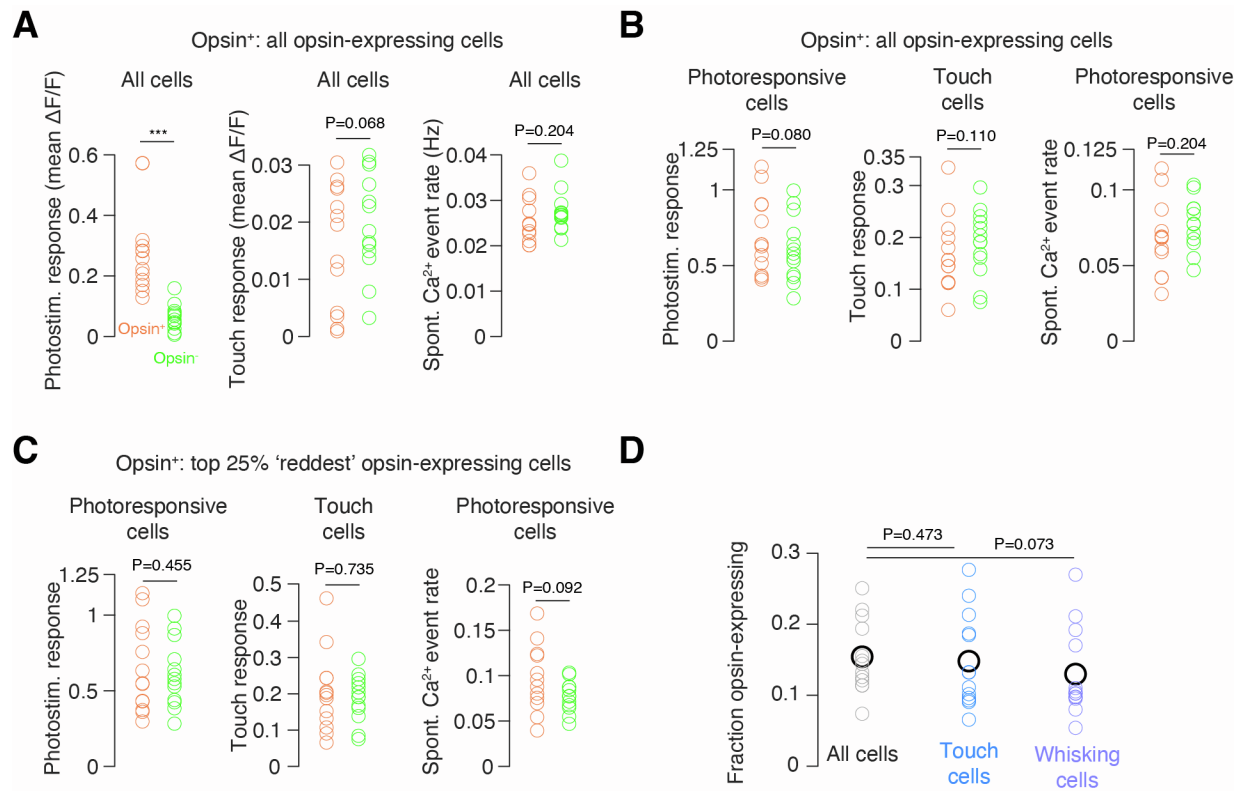
Figure S3. Comparisons of opsin-expressing and opsin non-expressing population activity, related to Figure 3.

(A) Comparison of all opsin-expressing and opsin non-expressing (Methods) neurons. Left, mean photostimulus-evoked ΔF/F for both populations on the first photostimulation session. Middle, mean touch-evoked ΔF/F for the first touch session, which occurred prior to any photostimulation (Methods). Right, mean calcium event rate during the inter-trial epoch ('spontaneous' event rate) during the first touch session. P-values are given for the paired Wilcoxon signed rank test comparing opsin-expressing and opsin non-expressing neurons (N=13 mice).

(B) As in A, but restricted to either the top 10% most photoresponsive neurons (for photoresponsiveness and spontaneous event rate) or top 10% most touch responsive neurons (for touch responsiveness). All opsin-expressing neurons are included.

(C) As in B, but the opsin-expressing population consists of the top 25% 'reddest' opsin-expressing neurons (Methods).

(D) Fraction of cell populations that were opsin-expressing. Gray, all cells. Blue, touch cells. Purple, whisking cells. P-values are given for Wilcoxon signed rank test comparing touch and whisking cell fractions with overall fraction.
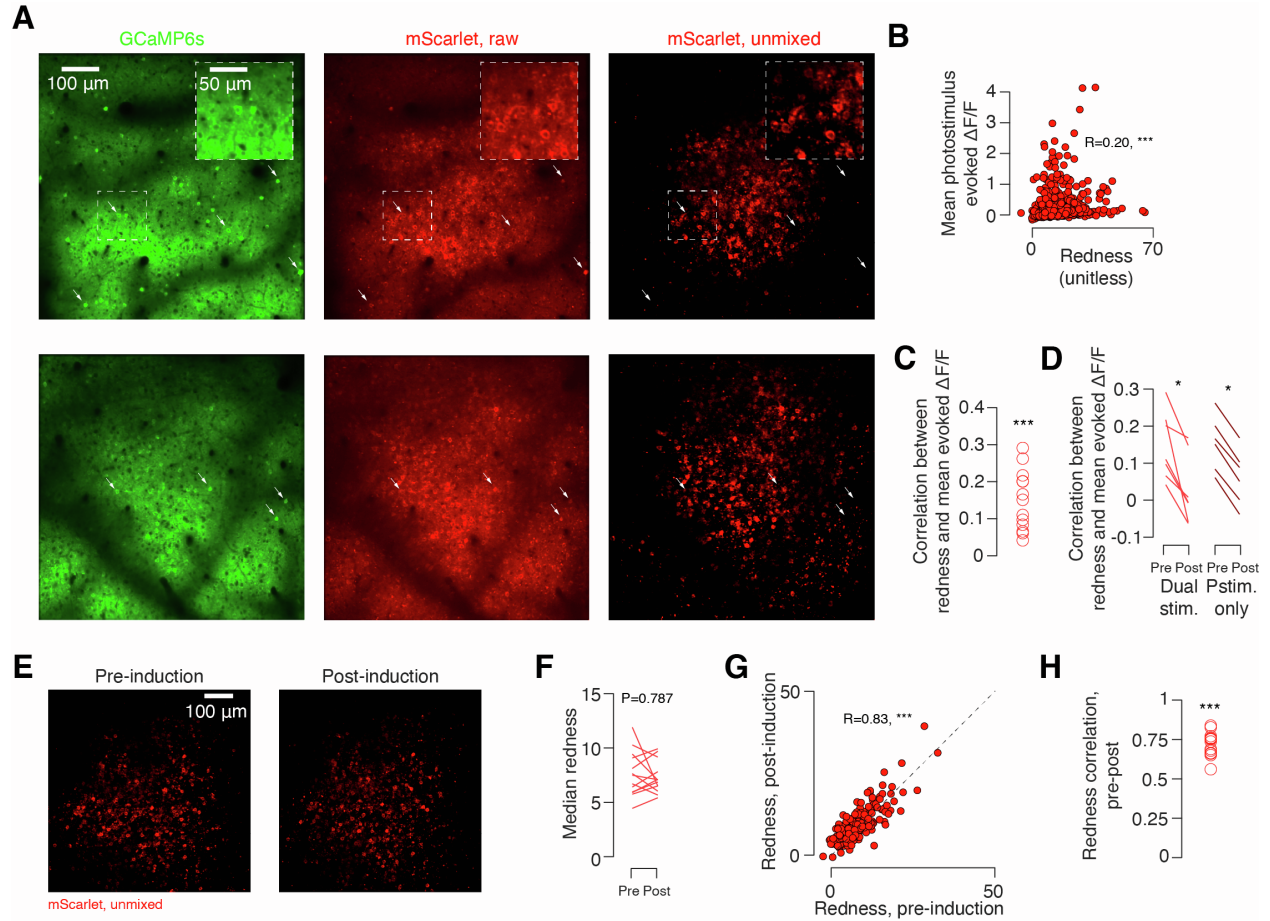
Figure S4. Influence of opsin expression levels on photostimulation response and stability of opsin expression, related to Figure 3.

(A) Opsin expression was assessed using the linearly unmixed red photomultiplier tube (PMT) channel image (Methods). Shown are two planes from two example mice (top, bottom). Left, raw GCaMP6s image from the green PMT channel. Middle, raw mScarlet image from the red PMT channel. Right, linearly unmixed mScarlet image – 'redness'. Arrows indicate neurons that appear to exhibit red fluorescence prior to unmixing.

(B) Relationship between redness of individual opsin-expressing neurons and the mean evoked ΔF/F following photostimulation. P-value indicated for Pearson correlation between redness and evoked ΔF/F. ***, $P < 0.001$; **, $P < 0.01$; *, $P < 0.05$.

(C) Pearson correlation between redness and evoked ΔF/F for all animals (N=13). P-value indicated for Wilcoxon signed rank test comparing the measured median to 0.

(D) Pre- and post-induction Pearson correlation between redness and evoked ΔF/F. Left, dual-stimulus induction. Right, photostimulation-only induction. P-value indicated for Wilcoxon signed rank test comparing pre vs. post-induction correlation, paired by animal.

(E) Linearly unmixed mScarlet image on the first and final days of induction in an example mouse.

(F) Median redness before and after induction. P-value for Wilcoxon signed rank test comparing pre- vs. post-induction redness, paired by animal (N=13). ***, $P < 0.001$; **, $P < 0.01$; *, $P < 0.05$.

(G) Pearson correlation between redness pre- vs. post-induction in an example animal. P-value given for Pearson correlation.

(H) Pearson correlation between pre- and post-induction redness for all animals. P-value indicated for Wilcoxon signed rank test comparing pre vs. post-induction correlation to 0, paired by animal.
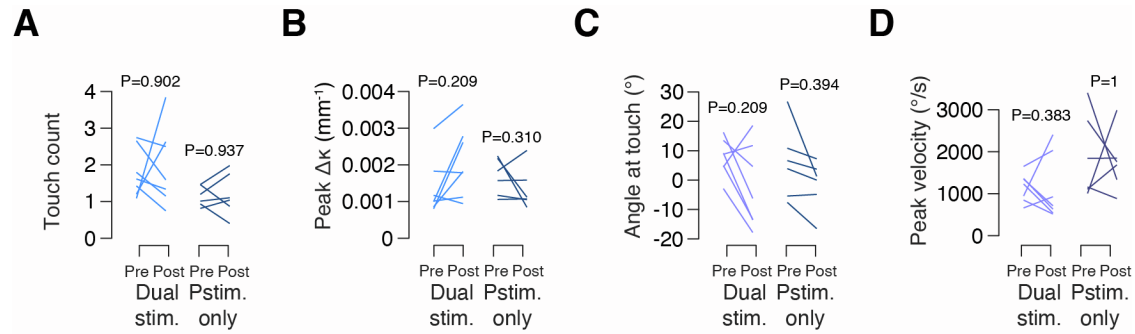
Figure S5. Vibrissal kinematics pre- and post-induction, related to Figure 5.
(A) Number of touches before and after induction, averaged across all trials in a session. Left, dual-stimulus induction. Right, photostimulation-only induction. P-value indicated for Wilcoxon signed rank test comparing pre vs. post-induction value, paired by animal.
(B) As in A, but for the peak curvature change (Δκ) experienced during a trial, averaged across trials.
(C) As in A, but showing the mean angle of the whisker at touch for a trial, averaged across trials.
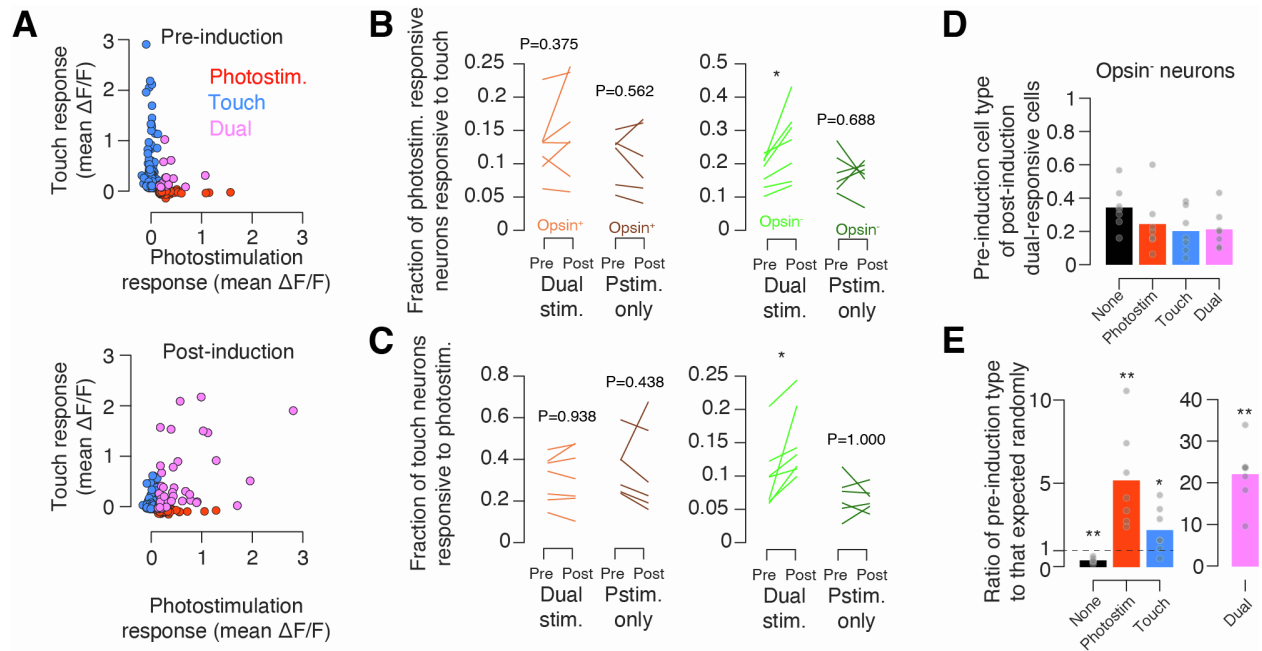(D) As in A, but showing the peak angular velocity during the trial, averaged across trials.

Figure S6. Basis of increased touch-photoresponsive population overlap following induction, related to Figure 5.

(A) Change in relationship between mean ΔF/F response to touch and photostimulation for all responsive opsin non-expressing neurons in an example mouse. Blue, neurons that belong only to the top 10% of touch responders; red, neurons that belong only to the top 10% of photostimulation responders; magenta, neurons that belong to both groups ('dual'). Top, relationship prior to induction. Bottom, relationship following induction.

(B) Fraction of photoresponsive neurons that also respond to touch before and after induction. Orange, opsin-expressing neurons; green, opsin non-expressing. Mice were exposed to dual-stimulus induction (lighter color, N=7 mice) or photostimulation-only induction (darker color, N=6 mice). P-values provided for signed rank test comparing fraction before and after induction. ***, P < 0.001; **, P < 0.01 ; *, P < 0.05.

(C) As in (B), but showing the fraction of touch responsive neurons that also respond to photostimulation.

(D) Fraction of neurons that were responsive to both photostimulation and touch following dual-stimulus induction having a given cell type prior to induction. Dots, individual animals. Bars, mean (N=7 mice).

(E) As in (D), but normalized to the size of each population on the post-induction day (i.e., what would be expected if neurons changed type randomly). P-values for signed rank test comparing the observed values to a distribution with median 0. ***, P < 0.001; **, P < 0.01; *, P < 0.05.
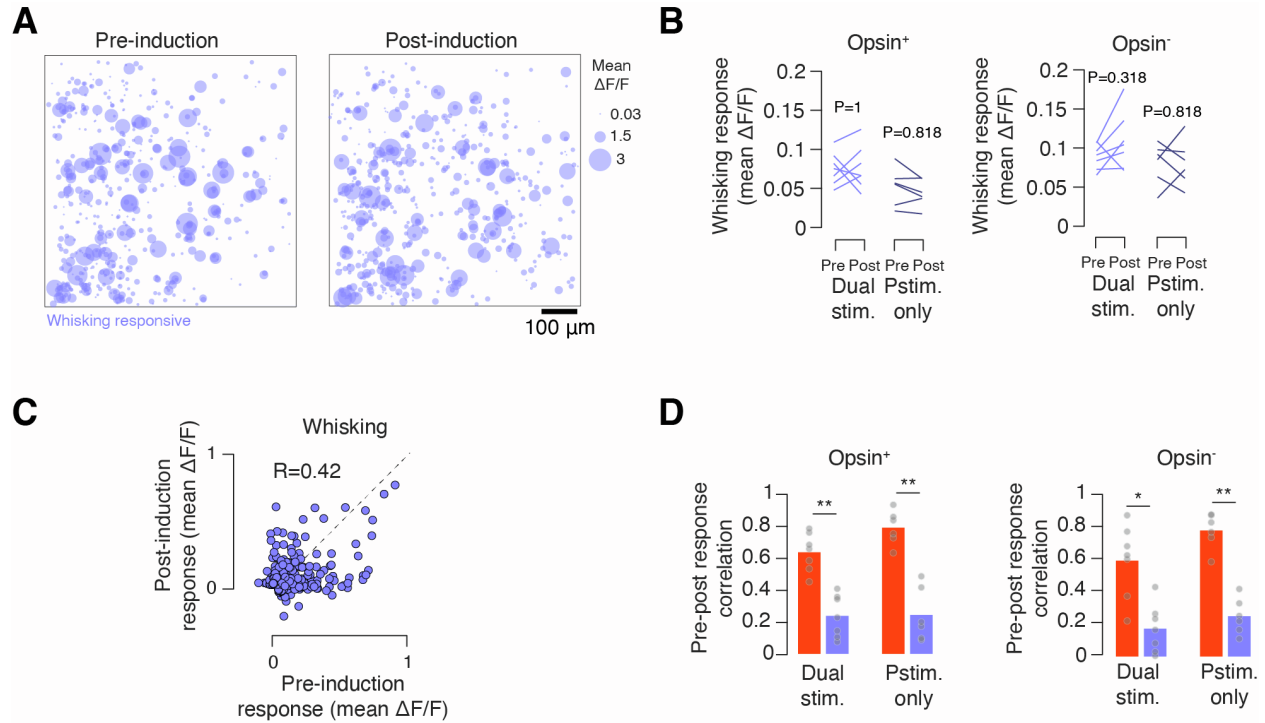
Figure S7. Change in whisking populations following induction, related to Figure 6.
(A) Whisking population in an example mouse before (left) and after (right) dual-stimulus induction. Neurons are collapsed across six planes spaced 20 μm apart. Colored circles show the mean whisking-evoked ΔF/F.

(B) Change in mean whisking-evoked ΔF/F among the top 10% of most whisking-responsive neurons following induction. Left, opsin-expressing; right, opsin non-expressing. In each case, we examined mice exposed to dual-stimulus induction (N=7; lighter color), and photostimulation-only induction (N=6; darker color). P-values provided for Wilcoxon signed rank test comparing response before and after induction. ***, P < 0.001; **, P < 0.01 ; *, P < 0.05.

(C) Whisking response (mean whisking onset-aligned ΔF/F) before and after dual-stimulus induction.

(D) Correlation of pre- and post-induction mean evoked ΔF/F for photostimulation responsive (red) and whisking responsive (purple) populations. Left, opsin-expressing; right, opsin non-expressing neurons. ***, P < 0.001; **, P < 0.01 ; *, P < 0.05; P-value for Wilcoxon signed rank test comparing whisking and photoresponsive populations.

Animal ID	Sex	Age at training start (d)	Opsin$^+$ cell count	Opsin$^-$ cell count	Induction protocol
an014261	M	97	1094	3461	Dual-stimulus
an014347	F	78	615	2950	Dual-stimulus
an014350	F	75	589	3529	Dual-stimulus
an015145	M	103	724	3304	Dual-stimulus
an014317	M	114	733	2358	Dual-stimulus
an016655	M	130	666	3652	Dual-stimulus
an017772	M	83	828	2257	Dual-stimulus
an014348	F	80	319	3002	Photostimulation-only
an015742	M	82	391	2137	Photostimulation-only
an015741	M	94	770	3165	Photostimulation-only
an016663	M	94	576	2363	Photostimulation-only
an015143	M	120	611	3145	Photostimulation-only
an014349	F	114	1012	2315	Photostimulation-only

Table S1. **List of animals, related to Figure 2**. All mice were transgenic Ai162 X Slc17a7-Cre, expressing GCaMP6s exclusively in excitatory neurons. All mice except an014261 were injected with 3 100 nL injections using a 1:500 dilution of AAV-8-CaMKIIa-ChRmine-mScarlet-Kv2.1-WPRE; an014261 received 1 20 nL injection with a 1:200 dilution.